HHS Public Access

Author manuscript

Sci Immunol. Author manuscript; available in PMC 2023 April 16.

Published in final edited form as:

Sci Immunol. 2023 January 06; 8(79): eabp9940. doi:10.1126/sciimmunol.abp9940.

Epithelial-intrinsic defects in TGFβR signaling drive local allergic inflammation manifesting as eosinophilic esophagitis

Karen Laky[1], **Jessica L. Kinard**[1], **Jenny Min Li**[1], **Ian N. Moore**[2], **Justin Lack**[3], **Elizabeth R. Fischer**[4], **Juraj Kabat**[5], **Rachel Latanich**[6], **Nicholas C. Zachos**[6], **Ajinkya R. Limkar**[7], **Katherine A. Weissler**[1], **Robert W. Thompson**[8], **Thomas A. Wynn**[8], **Harry C. Dietz**[9], **Anthony L. Guerrerio**[10,†], **Pamela A. Frischmeyer-Guerrerio**[1,†,*]

[1]Food Allergy Research Section, Laboratory of Allergic Diseases, National Institute of Allergy and Infectious Diseases, National Institutes of Health; Bethesda, MD 20892.

[2]Infectious Disease Pathogenesis Section, Comparative Medicine Branch, National Institute of Allergy and Infectious Diseases, National Institutes of Health; Bethesda, MD 20892.

[3]Collaborative Bioinformatics Resource, National Institute of Allergy and Infectious Diseases, National Institutes of Health; Bethesda, MD 20892 and Advanced Biomedical Computational Science, Frederick National Laboratory for Cancer Research, Frederick; MD 21701

[4]Electron Microscopy Unit, Research Technologies Branch, National Institute of Allergy and Infectious Diseases, National Institutes of Health; Hamilton, MT 59840.

[5]Biological Imaging Section, Research Technologies Branch, National Institute of Allergy and Infectious Diseases, National Institutes of Health; Bethesda, MD 20892.

[6]Department of Medicine, Division of Gastroenterology and Hepatology, Johns Hopkins University School of Medicine; Baltimore, MD, 21205.

[7]Inflammation Immunobiology Section, Laboratory of Allergic Diseases, National Institute of Allergy and Infectious Diseases, National Institutes of Health; Bethesda, MD 20892

[8]Immunopathogenesis Section, Laboratory of Parasitic Diseases, National Institute of Allergy and Infectious Diseases, National Institutes of Health; Bethesda, MD 20892.

[*]Corresponding Author: pamela.guerrerio@nih.gov.

[†]These authors contributed equally

Author contributions:

K.L., J.L.K., K.A.W., A.L.G, P.F.-G. conceptualized, designed, and conducted experiments, compiled data, and performed data analyses. The *Tgfbr1*^{M318R} Knock-In mouse model system originated in the lab of H.C.D. J.M.L. performed qPCR assays, compiled and analyzed the data. J.L. performed bioinformatic analyses of RNASeq samples. E.F. and J.K. performed and analyzed TEM analyses. A.R.L. performed transmigration assays, compiled and analyzed the data. I.N.M. performed immunohistochemistry staining and evaluated histological images. N.C.Z. and R.L. optimized the culture system for esophageal organoids and performed experiments. R.W.T. and T.A.W. optimized the assay for hydroxyproline quantification and performed experiments. Jingwen Gu (NIAID Bioinformatics Services) consulted on statistical analyses, K.L. and P.F.-G. wrote the manuscript with the help of all of the authors. P.F.-G., A.L.G., H.C.D. initiated and provided funding for the project.

Competing interests: Authors declare that they have no competing interests.

Supplementary Materials:

Fig. S1–S7.

Table S1–10.

MDAR reproducibility list

[9]McKusick-Nathans Institute of Genetic Medicine, Johns Hopkins University School of Medicine; Baltimore, MD 21205; Howard Hughes Medical Institute; Chevy Chase, MD 20815, USA.

[10]Department of Pediatrics, Division of Gastroenterology, Hepatology, and Nutrition, Johns Hopkins University School of Medicine; Baltimore, MD 21287

Abstract

Allergic diseases are a global health challenge. Individuals harboring loss-of-function variants in transforming growth factor beta receptor (TGFβR) genes have an increased prevalence of allergic disorders, including eosinophilic esophagitis. Allergic diseases typically localize to mucosal barriers, implicating epithelial dysfunction as a cardinal feature of allergic disease. Here, we describe an essential role for TGFβ in the control of tissue-specific immune homeostasis that provides mechanistic insight into these clinical associations. Mice expressing a TGFβR1 loss-of-function variant identified in atopic patients spontaneously develop disease that clinically, immunologically, histologically, and transcriptionally recapitulates eosinophilic esophagitis. *In vivo* and *in vitro*, TGFβR1 variant-expressing epithelial cells are hyperproliferative, fail to differentiate properly, and overexpress innate pro-inflammatory mediators, which persists in the absence of lymphocytes or external allergens. Together, our results support the concept that TGFβ plays a fundamental, non-redundant, epithelial cell-intrinsic role in controlling tissue-specific allergic inflammation that is independent of its role in adaptive immunity.

One Sentence Summary:

TGFβ is an essential non-redundant epithelial cell-intrinsic controller of allergic inflammation independent of its role in adaptive immunity.

Eosinophilic Esophagitis Essentials

Individuals with loss-of-function variants of transforming growth factor beta receptor (TGFβR) genes develop allergic diseases including eosinophilic esophagitis (EoE), but mechanisms driving disease pathology are not well understood. Here Laky et al. define an essential role for TGFβR in maintaining epithelial cell homeostasis to control allergic inflammation. Mice bearing TGFβR1 loss-of-function variants developed disease symptoms consistent with EoE, which was reflected in pathological, immunological, and transcriptional changes to esophagus. Expression of TGFβR1 variants in epithelial cells was associated with hyperproliferation, defects in differentiation, and the release of pro-inflammatory mediators, even in the absence of allergens or lymphocytes. These findings highlight an epithelial-cell intrinsic function of TGFβR1 in modulating allergic inflammation associated with EoE.

INTRODUCTION

Allergic diseases are among the most pervasive medical conditions to affect humans, and their prevalence is rising at a dramatic rate. The factors that initiate allergic inflammation and confer the tissue specificity characteristic of allergic conditions remain obscure. As the interface with the external environment, epithelial cells are the first to encounter allergens and play a pivotal role in maintaining immune homeostasis, but the mechanisms and

pathways involved are incompletely understood. It has been proposed that a leaky epithelial barrier causes allergic disease by allowing penetration of antigens that then instigate an inflammatory immune response. In addition to providing a physical impediment to external insults, epithelial cells promote local immune responses and tissue repair that, if unchecked, can induce pathology. Even though epithelial dysfunction is a feature of nearly all allergic diseases, whether it is a primary inciting event or a consequence of an aberrant immune reaction is not clear.

Eosinophilic esophagitis (EoE) is a chronic disease characterized by eosinophilic inflammation in the esophagus, typically manifesting in patients as dysphagia and food impaction. EoE shares many features in common with other allergic disorders, including characteristics of the inflammatory cell infiltrate, the presence of epithelial hyperplasia, and the induction of epithelial-derived alarmins, suggesting a shared pathophysiology. Both environmental and genetic factors contribute to the pathogenesis of EoE. Among the top 10 gene variants linked to EoE, nearly all occur in genes expressed by epithelial cells, and approximately 1/3 encode proteins involved in transforming growth factor beta (TGFβ) signaling (1). We previously reported that patients with Loeys-Dietz syndrome who harbor loss-of-function variants in genes encoding the receptor for TGFβ (*TGFBR1, TGFBR2*) are more likely to develop allergic diseases, including EoE (2). To investigate the mechanisms by which diminished TGFβR signaling promotes localized allergic inflammation in EoE, we utilized mice with the $Tgfbr1^{M318R}$ (R1) variant knocked into the endogenous *Tgfbr1* locus (3). This variant is a point mutation that results in expression of TGFβR1 devoid of kinase activity (4).

We find that R1 mice spontaneously develop EoE that closely recapitulates the human disease with 100% penetrance, and we demonstrate that a primary defect in epithelial development, independent of lymphocytes or allergens, can initiate a Th2 inflammatory cascade. Decreased TGFβR signaling in esophageal epithelial cells leads to an ineffective cytostatic differentiation program, resulting in excessive proliferation and secretion of pro-inflammatory mediators. We propose the origin of allergic disease to be local sterile inflammation initiated by epithelial cells, expanding the role of epithelium beyond barrier function to include its innate immune functions in the allergic disease diathesis. These findings advance our understanding of the mechanisms that normally limit tissue-specific allergic inflammation.

RESULTS

R1 mice spontaneously develop disease that meets the diagnostic criteria for EoE

The most common presenting symptoms in patients with EoE are dysphagia and food impaction. While the esophagi of wild type (WT) mice (Fig. 1A) were narrow and empty, the esophagi of R1 mice were enlarged (Fig. 1B) and more solid material was recovered after flushing esophagi of R1 than WT mice (Fig. 1C). Dilation and impacted food were also evident in cross-sections of esophageal tissue from R1 mice (Figs. 1D to G). In addition to esophageal dysfunction, a diagnosis of EoE requires the presence of ≥15 eosinophils per high powered field. Intact and degranulated eosinophils in R1 esophagi were visualized by immunohistochemical (IHC) staining of the eosinophil granule protein major basic protein

1 (MBP) (Figs. 1F to J). Eosinophils were rare in WT esophageal tissue (Fig 1F) and a single layer of nucleated basal cells was present (Fig 1K). Additional histological features characteristic of EoE (5) observed in R1 esophagi included basal cell hyperplasia (Fig. 1L–N), eosinophilic abscesses (Figs. 1I, M), surface layering of eosinophils (Fig. 1J) and rete peg elongation (Figs.1E, M, N). Thus, the clinical and histological features of R1 esophagi satisfy the established diagnostic criteria for EoE.

The esophageal transcriptome, inflammatory infiltrate, and age of disease onset in R1 mice phenocopies EoE endotype 2

A combination of gene expression changes, clinical characteristics, and histopathological findings can be used to diagnose several endotypes of EoE (6, 7). To determine the degree of similarity between R1 mice and human disease endotypes, we performed RNAseq on tissue from the inner esophagi of R1 mice and calculated correlation coefficients between the gene expression levels in our mouse samples and the mean expression of each endotype from the human discovery cohort of Shoda et al (7). R1 mice have enrichment for genes differentially expressed in endotype 2 (EoEe2), and an inverse correlation with endotype 3 (EoEe3) (Fig. 2A). RT-PCR analyses confirmed that R1 esophagi had higher expression of *Tslp* and *Tnfaip6,* the 2 genes most uniquely associated with EoEe2 (Fig. 2B).

A physical feature that distinguishes endotypes is the absence of fibrosis in EoEe2 and presence of fibrostenosis in EoEe3. *COL8A2* is the representative collagen gene in the human EoE diagnostic panel, and its upregulation distinguishes EoEe2 and EoEe3 from EoEe1 (7). Expression of *Col8a2* was significantly higher (P=0.0001) in R1 esophagi than WT littermates (Fig. 2C). However, R1 mice did not have narrow esophagi and the most highly expressed collagen genes were lower in R1 than WT esophagi, including several collagen genes known to be upregulated in response to TGFβ (8). These *ex vivo* data were consistent with *in vitro* data that show induction of SMAD target genes is impaired in cells transfected with the $Tgfbr1^{M318R}$ variant (4). Collagen expression at the protein level was visualized with Masson's Trichrome stain (Fig. 2D) and quantified by measuring hydroxyproline (Fig. 2E) (9). There was no increase in collagen in R1 esophagi compared to WT mice.

We then expanded our gene expression analyses beyond the EoE diagnostic gene panel. Of $\times 6 \times 10^4$ genes detected, 2.7×10^3 genes were differentially expressed (Fig. S1). Among those differentially expressed genes, 6% differed >2-fold, the cutoff established for the human EoE transcriptome (6). Like data sets generated with human biopsies (10, 11), most differentially expressed genes were higher in R1 than WT esophagi. Upregulated pathways in R1 esophagi were related to immune responses and included genes involved in eosinophil cytokine/chemokine signaling, adhesion, and granule proteins; mast cell effector proteins; T cell activation, adhesion, and cytokine signaling, and myeloid cell recruitment and activation (Fig. 3A). The cell lineages represented in this pattern suggest an inflammatory infiltrate reminiscent of human EoE (12, 13).

We corroborated our gene expression data by using flow cytometry to quantify the number of total leukocytes, and eosinophils specifically, that were present in WT and R1 esophagi from mice of various ages (Figs. 3B, C, and S2). The identity of eosinophils was confirmed

by modified Giemsa staining of $CD11b^{+}SiglecF^{+}$ cells purified from R1 esophagi (Fig. 3D). Esophageal dilation and increased eosinophils were already present in esophagi of R1 pups at weaning (Figs. 3C, E–G), consistent with the pediatric-onset of EoEe2. In addition to eosinophils, the inflammatory infiltrate in R1 esophagi included more myeloid antigen presenting cells (mAPCs), mast cells, type 2 ILCs (ILC2s), and T cells (Fig. 3H), recapitulating the infiltrate observed in patient biopsies (14–16). Consistent with recent flow cytometry and single cell gene expression data from human biopsies, B cells, basophils, granulocytes, and natural killer cells were few in number in both WT and R1 esophagi (Fig. S3) (12, 13). No gross alterations in the frequency of lymphoid or myeloid subsets was noted in blood, spleen, or thymus of R1 mice (Table S1). Mice harboring a loss-of-function variant in TGFβR2 (*Tgfbr2*$^{G357w/+}$) also spontaneously develop EoE (Fig. S4). Taken altogether, the age of onset, transcriptome, clinical features, histological features, and inflammatory infiltrate of mice with defective TGFβR signaling recapitulates human EoEe2.

EoE phenotype caused by the R1 variant is not lymphocyte dependent

TGFβ is a negative regulator of T cells (17), which have been posited to be the primary drivers of inflammation in EoE. To determine how T cells contribute to EoE pathology in R1 mice, we introduced the R1 variant into mice congenitally lacking lymphocytes. Surprisingly, despite a complete absence of T cells, $RAG2^{-/-}$R1 esophagi had increased eosinophils, mast cells, mAPCs, and ILC2s (Fig. 3H) and the numbers were comparable to RAG2-sufficient R1 mice. In addition to accumulation of eosinophils, $RAG2^{-/-}$R1 mice developed hallmark clinical and histological features of EoEe2, including esophageal dilation with food impaction (Figs. 3I–K), basal cell hyperplasia (Figs. 3L, M), and MBP^{+} cells (Figs. 3N, O). In summary, no aspect of the EoE phenotype caused by the R1 variant was lymphocyte dependent.

Radio-resistant non-hematopoietic cells are necessary and sufficient to cause an EoE phenotype in R1 mice

The development of EoE in $RAG2^{-/-}$ R1 mice excluded ineffective inhibition of T cells by TGFβ as the cause of EoE. TGFβRs are ubiquitously expressed. To assess the relative contributions of altered TGFβR signaling in bone marrow (BM)-derived versus non-hematopoietic cells to EoE pathophysiology, R1 mice were irradiated and reconstituted with WT BM. Eight weeks post-reconstitution, WT donor BM-derived eosinophils had accumulated in the esophagi of R1 mice (Fig. 4A) accompanied by esophageal dilation and food impaction (Fig. 4B). This was true for R1 mice irradiated and reconstituted as adults with established disease, or as neonates prior to the onset of disease. In the converse experiment, WT mice irradiated and reconstituted with R1 BM did not develop features of EoE (Figs. 4C, D). Thus, attenuated TGFβR1 signaling in radio-resistant host cells was necessary and sufficient to cause EoE in R1 mice. To the contrary, altered TGFβR1 signaling in BM-derived cells alone did not cause disease.

Diminished TGFβR signaling leads to tissue restricted allergic inflammation

A diagnostic criterion of EoE is that eosinophilic inflammation is isolated to the esophagus (18). A survey of tissues confirmed that eosinophils were not increased in BM, lymphoid organs, or intestines of R1 mice (Fig. 4E). One striking exception was stomach. Unlike in

humans, the proximal forestomach in mice is lined by stratified squamous epithelium that is contiguous with the esophagus up to the limiting ridge. The distal glandular stomach and intestines are lined by simple columnar epithelium. When proximal and distal portions of the stomach were analyzed separately, eosinophils were noticeably increased only in forestomach. The forestomach of R1 mice also exhibited the same histopathological features as the esophagus, namely basal cell hyperplasia, eosinophilic abscesses, and rete peg elongation with peripapillary accumulation of eosinophils (Figs. 4F to I). The adjacent glandular stomachs of R1 and WT mice were indistinguishable. The observation that accumulation of eosinophils in R1 mice was anatomically limited to tissues lined by stratified squamous epithelium suggested to us that these specialized cells were responsible for the tissue-restricted inflammation.

EoE in R1 mice is not predicated on altered esophageal barrier function

We sought to understand the mechanisms by which epithelium could drive allergic inflammation. Because it has been proposed that a leaky epithelial barrier causes EoE by allowing penetration of antigens that then instigate an inflammatory response (19), we examined expression of genes encoding proteins that contribute to epithelial barrier function (Fig. 5A, ●). In healthy differentiating keratinocytes, genes encoding involucrin (*IVL*), envoplakin (*EVPL*), and periplakin (*PPL*) are induced concurrently, followed by filaggrin (*FLG*) and loricrin (*LOR*), and desmoglein 1 (*DSG1*) (19, 20). *Ivl* and *Evpl* expression were higher in R1 than WT esophagi, but *Ppl* was lower in R1 than WT. Expression of *Flg* did not differ between WT and R1 esophagi, but *Lor*, *Dsg1a,* and *Dsg1b* were lower in R1 than WT. Discordant expression of genes that are typically co-expressed suggested that differentiation of R1 epithelial cells was perturbed.

To determine if the gene expression changes observed impacted intercellular contacts, we examined the architecture of the esophageal epithelium using transmission electron microscopy. The suprabasal layers of epithelium of WT and R1 esophagi were indistinguishable (Fig. 5B–J). Stratum corneum consisted of interlocking fibers that excluded luminal contents. Stratum granulosum contained flat, tightly packed cells interconnected by evenly spaced desmosomes around the perimeter of each cell. Stratum spinosum contained nucleated cells transitioning from cuboidal to flat and interconnected by desmosomes between spiny projections. Neither dilated intercellular spaces (ICS) nor changes in the number, distribution, or structure of desmosomes were observed in the suprabasal strata.

In contrast to the suprabasal layers, substantive differences between R1 and WT esophagi were present in the stratum basale. Whereas this layer consisted of only 1–2 cuboidal cells in WT esophagi (Fig. 5K) R1 epithelium contained areas that were several cells thick, indicative of basal cell hyperplasia (Figs. 5L). At a cellular level, WT basal cells were characterized by a network of microvillar projections, well-defined nuclei with diffuse chromatin, and abundant mitochondria (Fig. 5N). In contrast, R1 basal cells (Figs. 5O, P) displayed clubbing, loss of microvillar projections, nuclei with tightly compacted chromatin, increased nucleus:cytoplasmic ratio, and a paucity of mitochondria, suggesting that basal cells in R1 esophagi were distressed and displaying ultrastructural features of pyroptosis.

Eosinophils were seen adjacent to R1 basal epithelial cells (Figs. 5M, Q). Clubbing can give the appearance of dilated ICS, but there was no difference in the mean distance between cell bodies of adjacent epithelial cells in the stratum basale of WT and R1 mice (Figs. 5U and S5). Thus, the ultrastructural features of R1 esophageal epithelium match pediatric patients with active EoE (21).

To determine whether the differences in gene expression and ultrastructural features in R1 mice led to a leaky esophageal barrier, we assessed barrier function. Transepithelial electrical resistance (TEER) was used to quantitate the electrical impedance of esophageal tissue (Fig. 5R). We also measured paracellular transport of molecules comparable in size to common food allergens (Figs. 5S, T). Minimal permeability was observed using either assay, and there were no differences between WT and R1 tissues. Thus, disruption in esophageal barrier function could not explain the development of EoE in R1 mice.

Decreased TGFβR signaling leads to excessive proliferation and impaired differentiation of epithelial cells

Because esophageal barrier function was intact, we asked what other mechanisms could be driving inflammation in R1 esophagi. A closer look at the gene expression pattern of structural genes revealed that the transcriptional profile of R1 esophagi was enriched for genes seen in immature epithelial cells, at the expense of genes characteristic of differentiated cells. For example, immature epithelial cells express mainly *Cdh3*, and as cells differentiate, they downregulate *Cdh3* and begin to express *Cdh1* which encodes E-cadherin (22). Expression of *Cdh3* was higher and *Cdh1* lower in R1 compared to WT esophagi (Fig. 5A, ◄). Similarly, *Cldn4,* which is expressed by mature keratinocytes, was decreased while *Cldn1,* which is expressed by immature epithelial cells, was increased (Fig. 5A, ←). The promoters for *Cdh1, Cdh3, Cldn1* do not contain canonical SMAD binding motifs suggesting that their dysregulation in R1 epithelial cells is indirect.

Keratin genes are tightly regulated during development and can be used to evaluate keratinocyte differentiation. Basal cell *Krt14* was increased whereas *Krt13* and *Krt78*, which are expressed by differentiated keratinocytes, were decreased in R1 esophagi (Fig. 5A,*). IHC validated that keratin 14 (K14) protein was more highly expressed in R1 esophagi and revealed that its localization differed markedly from WT esophagi (Figs. 6A, B). As expected, K14 in WT esophagi was restricted to a thin layer of basal cells. R1 esophagi had abnormal persistence of K14 far beyond the basal layer. Dysregulated expression of keratins and E-cadherin is also seen in patients with EoE (23, 24).

We went on to compare expression of genes that are the most differentially expressed between differentiated and basal keratinocytes (25). Interestingly, numerous genes used to characterize keratinocyte maturation are targets of TGFβ-mediated regulation. In addition to structural genes, other genes were reciprocally dysregulated in R1 esophagi, with basal cell genes upregulated and differentiated keratinocyte genes downregulated. Among the most strikingly increased were genes encoding the epithelial stem cell amino acid transporter *Slc1a3*, epidermal growth factor receptor ligand *Areg,* and the transcription factor *Ets1* (Fig. 6C and Tables S2, S3). Overexpression of Ets1 inhibits keratinocyte differentiation and induces a stress response (26). Increased *Ets1* in R1 esophagi was accompanied by induction

of stress keratin 6 (Figs. 6D, E), verifying that differentiation of R1 epithelial cells was aberrant.

Many of the genes characteristic of immature keratinocytes reflect the proliferative nature of basal cells (Table S3). Among the genes higher in R1 than WT esophagi (Fig. 6C) were several that encode proteins involved in proliferation and DNA replication, including proliferating cell nuclear antigen (*Pcna*), which is used to visualize basal cells in biopsy sections. In many cell types, including the human esophageal epithelial cell line HET1a, TGF-β induces cell cycle arrest (27). We confirmed that primary murine esophageal epithelial cells expressed *Tgfbr1*, that the level of phosphorylated SMAD2/3 was lower in R1 than WT esophageal epithelial cells directly *ex vivo*, and that induction of pSMAD2/3 in R1 esophageal epithelial cells in response to recombinant TGFβ *in vitro* was compromised on a per cell basis (Fig. S6). We then looked at expression of cell cycle related genes that are modulated at the transcriptional level by TGFβ *in vitro* (Fig. 6F and Tables S4, S5) (28–30). Expression of genes encoding proteins that promote proliferation and DNA replication were higher in R1 esophagi than WT. Conversely, genes encoding proteins that inhibit proliferation and promote differentiation were lower in R1 than WT esophagi. Canonical TGFβ target genes that were differentially expressed included inhibitor of differentiation (*Id*), growth arrest and DNA damage inducible (*Gadd*), growth arrest specific (*Gas*), cyclin dependent kinase (*Cdk*), CDK regulatory genes (*Cdkn, Cdc*), and the proto-oncogene *Myc*. Thus, the transcriptome of R1 esophagi suggested aberrant cell cycle regulation.

Much of cell cycle regulation occurs at the post-translational level. To determine if the gene expression changes induced by the $Tgfbr1^{M318R}$ variant culminated in increased proliferation of epithelial cells *in vivo*, R1 and WT mice were pulsed with the thymidine analogue bromodeoxy-uridine (BrdU). After 24 h, cells with nuclear BrdU indicating that they had recently passed through the S phase of the cell cycle, were visualized (Figs. 6G to N). Scattered $BrdU^+$ cells were seen in a single layer of WT esophagi (Fig 6G), whereas esophagi of R1 mice had a greater frequency of $BrdU^+$ epithelial cells (Fig. 6H). Increased $BrdU^+$ epithelial cells were also evident in the forestomach (Figs. 6I–L), but not glandular stomach (Figs. 6M, N), of R1 mice. These data show that reduced TGFβR signaling in squamous epithelial cells impaired cell cycle regulation, manifesting as basal cell hyperplasia, which is a prominent histological feature of EoE (5, 31).

Epithelial cells in R1 esophagi initiate an inflammatory cascade

Collectively, our findings demonstrate an accumulation of immature, hyperproliferating, and distressed epithelial cells in R1 esophagi. We sought to identify mechanisms by which these TGFβ-induced perturbations in epithelial cell homeostasis could lead to inflammation. Although most differentiated keratinocyte genes were lower in R1 than WT esophagi, *Il1r1* and C*asp1* were upregulated in R1 basal cells (Fig. 6C). Secretion of preformed IL-1α is an innate immune mechanism by which distressed epithelial cells rapidly initiate local inflammatory responses that are subsequently amplified and prolonged by induction of IL-1β and TNFα (32, 33). *Il1b* and *Tnf* were upregulated in R1 esophagi (Fig. 7A). Moreover, R1 esophagi had an inflammatory signature indicative of chronic activation by IL-1 and TNFα (Fig. 7A and Tables S6, S7) (32, 34–38). The inflammatory cascade at

barrier surfaces is intended to protect against infectious agents and promote wound healing. IL-1 induced genes that were higher in R1 than WT esophagi included keratinocyte growth factors, complement components, cytokines, chemokines, and adhesion molecules (Fig. 7A). *Ccl17, Ccl22*, and *Vcam* were among the most highly upregulated genes. CCL17 and CCL22 attract $CCR4^+$ T cells, ILC2s, mAPCs, and eosinophils (39, 40) whose entry into tissues is facilitated by vascular cell adhesion molecule expression on endothelial cells (41–43). Damage associated molecular pattern molecules (DAMPs) increased in R1 esophagi included *Il1b,* defensins, serum amyloid, chitinase-like, and S100 proteins (44, 45).

Several molecules characteristic of allergic inflammation and epithelial hyperproliferation were selected for further investigation at the protein and anatomic levels (Figs. 7B–I and S7). *In vivo*, expression of S100A9 reflects abnormal keratinocyte development and *in vitro*, TGFβ suppresses expression of S100A9 by keratinocytes (46). Epithelial cells containing low levels of S100A9 were occasionally seen in WT esophagi (Fig. 7B). and stomach (Fig. D). In R1 mice, S100A9 protein was abundant in esophagus (Fig. 7C) and forestomach (Fig. 7E) epithelium and hematopoietic cells in the lamina propria, consistent with the increased number of eosinophils and mAPCs enumerated by flow cytometry (47). Cells expressing eosinophil chemotactic factor like protein (ECF-L, YM1/2, CHI3L3/4) were concentrated in the subepithelial layer of esophagi and limiting ridge of WT mice (Figs. 7F, H) (48, 49). High levels of ECF-L were present throughout the suprabasal epithelium and lamina propria of esophagi (Fig. 7G). and forestomach of R1 mice (Fig. 7I). Induction of DAMPS was not seen in intestine or esophageal muscle (Figs. 7B–I and S7). The observation that eosinophils and DAMPs colocalized in tissues lined by stratified squamous epithelium is compelling evidence that attenuated TGFβR signaling in these specialized epithelial cells is responsible for the tissue-restricted eosinophilic inflammation in R1 mice. Thus, although the esophageal epithelium was structurally intact in R1 mice, diminution of TGFβR signaling led to activation and altered immunocyte function of squamous epithelial cells.

Esophageal epithelial cells with reduced TGFβR signaling secrete immune mediators with chemotactic activity

The ability of non-hematopoietic cells to drive disease in BM chimeras coupled with co-localization of eosinophilic inflammation and activated epithelial cells in unmanipulated R1 mice argued that decreased TGFβR signaling in squamous epithelium was central to EoE pathogenesis. However, gene expression changes in *ex vivo* esophageal tissue reflect the sum of altered TGFβR signaling in many cell types. To begin to identify transcriptional changes caused by the R1 variant that were intrinsic to epithelial cells, organoids were initiated using stem cells from the epithelium of R1 and WT esophagi (Fig. 8A). Organoids recapitulated many EoE features including elevated expression of EoEe2 signature genes (Fig. 8B), increased expression of factors that promote epithelial proliferation (Fig. 8C), and hyperproliferative basal cells (Fig. 8D).

Consistent with gene expression data from EoE esophageal tissue (Fig. S1 and (10, 11)) most of the differentially expressed genes we examined were higher in R1 than WT organoids. Cytokine genes that were increased in R1 esophagi *ex vivo* and also higher

in R1 than WT organoids included IL-1 family members, TNFα, and numerous chemokines. Two of the most highly induced chemokine genes in R1 esophagi were *Ccl22* and *Ccl5* (Fig. 8E). *Ccl22*, which encodes stimulated T cell chemotactic protein 1 (50), and *Ccl5*, which encodes RANTES, were each ×7-fold higher in R1 organoids than WT. Increased secretion of RANTES by esophageal epithelial cells was confirmed by measuring its concentration in R1 or WT organoid culture supernatants (Fig. 8F). Similarly, increased *Csf2* translated to more GM-CSF secretion by R1 organoids than WT (Fig. 8F). However, not all *in vivo* changes were replicated *in vitro.* For example, *Ccl2* and *Ccl8* were increased ≥4-fold in esophageal tissue from R1 mice as compared to WT mice *ex vivo* but did not differ *in vitro* (Fig. 8E). This is consistent with data from patient biopsies in which *CCL2* is highly expressed by mast cells and fibroblasts, but not epithelial cells (51). Thus, although not absolutely required, non-epithelial innate cells likely also contribute to EoE pathology *in vivo*.

C3, CCL5, CCL17, TNFα, and GM-CSF can each attract eosinophils and were higher in R1 than WT organoids (Figs. 8E, F) (39, 42, 52, 53). To confirm that R1 esophageal epithelial cells secrete factors capable of recruiting eosinophils, media conditioned by organoids was used in transwell migration assays (Fig. 8G). Media conditioned by R1 epithelial organoids recruited more eosinophils than media from WT organoid cultures. Thus, attenuated TGFβR signaling was sufficient to induce cell-intrinsic defects in epithelial cells that reproduced *in vitro* the cardinal features of allergic inflammation, namely basal cell hyperplasia, altered gene expression, and eosinophil recruitment. Collectively, our data suggest that impaired TGFβR signaling in epithelial cells leads to epithelial distress and local release of immune mediators that are capable of driving the activation and expansion of other tissue resident cells and promoting the recruitment and activation of innate and adaptive immune cells.

DISCUSSION

The prevalence of allergic disease has escalated at an unprecedented rate in recent years, necessitating a deeper understanding of the pathways and mechanisms responsible. Using mice expressing a *Tgfbr1* variant that predisposes to allergic disease in humans as a model system, we have identified TGFβR signaling as an essential and non-redundant regulator of tissue homeostasis that protects against pathologic type 2 immune responses. Perturbation of this signaling pathway recapitulated the inflammatory infiltrate, histologic findings, gene expression changes, and clinical features characteristic of human EoE. Remarkably, the mechanisms driving disease were epithelial-cell intrinsic and occurred in the absence of lymphocytes or external stimuli. TGFβ has long been recognized to play a critical role in maintaining tolerance via effects on cells of the adaptive immune system (17). Our work reveals a fundamental role for TGFβ in maintaining immune homeostasis and preventing tissue-specific allergic inflammation via direct effects on non-hematopoietic cells. We shed light on the unique and complex biology of esophageal epithelial cells by demonstrating that cell-intrinsic defects that affect their differentiation are sufficient to start an innate immune cascade that leads to allergic inflammation. Furthermore, our work demonstrates that dysfunction in a single gene can lead to the cardinal manifestations of allergic disease: the inflammatory infiltrate, histologic findings, gene expression changes, and clinical features.

An important concept to emerge from our results is that allergic inflammation, and specifically EoE, can be initiated and sustained by epithelial-derived mediators independent of the adaptive immune system. We propose that esophageal epithelial cell distress, caused in part by aberrant differentiation and excessive proliferation, is an initiating event in a chronic inflammatory cascade (33, 54, 55). Our data suggest several ways in which clinical features of EoE can develop independent of the adaptive immune system. Expression of *Tnf* and *Il1b* by R1 esophageal epithelial cells is elevated, and both cytokines can influence esophageal smooth muscle contraction resulting in dysphagia and food impaction (56). In response to epithelial-derived DAMPs, tissue resident innate immune cells proliferate, accumulate, and secrete chemokines and cytokines creating a positive feedforward amplification loop (57). Keratinocytes express S100s, which are ligands for RAGE (34). IL-1, IL-33, and TNFα stimulate expansion and cytokine secretion by ILC2s that drive further epithelial proliferation, activate myofibroblasts, and alter endothelial cell gene expression (58–61). Stem cell factor is a growth and activation factor for Kit^+ mast cells and ILC2s, which contribute to asthma and anaphylaxis (62). ILC2s, mast cells, eosinophils, macrophages, and dendritic cells respond to IL-33 (63–65). In patients with active EoE, $IL\text{-}33R^{high}$ activated mast cells in the esophagus express high levels of *IL5, IL13, CCL2, CSF1, AREG*, and *VEGF* (51). Furthermore, mast cell-derived mediators can cause tissue damage, smooth muscle remodeling, and upregulation of adhesion molecules (14, 66–68). Cumulatively, tissue damage, local accumulation of inflammatory mediators, increased adhesion molecule expression, and mechanical changes facilitate recruitment, extravasation, proliferation, and activation of eosinophils, mast cells, ILC2s, APCs, and T cells as well as esophageal dysfunction – the hallmarks of EoE.

Our model bears similarity to previous models in that it places epithelium at the center of the EoE diathesis. However, our model differs substantively from others in that our data do not support the notion that EoE is caused by an immune response against food antigens that cross a leaky esophageal epithelium. Eosinophilic inflammation and esophageal dysfunction developed in R1 mice even though suprabasal esophageal epithelial strata were structurally intact and impermeable to particulates. Moreover, R1 epithelial cells were hyperproliferative and secreted chemokines *in vitro*. Although evidence suggests that exposure to antigens through damaged skin promotes food allergy, there is little convincing evidence that exposure to antigens through a leaky esophageal barrier leads to EoE. Antigen-induced mouse models of EoE rely on sensitization to antigen at peripheral sites, not *in situ* in the esophagus. Cutaneous, intranasal, or intraperitoneal administration of antigen induces esophageal eosinophilia, but oral or intragastric administration of antigen does not (69–72). Thus, we favor the hypothesis that in cases where esophageal barrier integrity is impaired, it occurs as a consequence of prolonged inflammation and epithelial cell distress (21, 73). In support of this hypothesis, functional changes in permeability and barrier gene expression are recapitulated by treatment of WT esophageal epithelial cells with exogenous IL-13 (74, 75), arguing that barrier changes are secondary to type 2 cytokine secretion.

Most current models assert that Th2 cytokines secreted by CD4 T cells responding to food antigens initiate EoE. T cells are increased in the esophagi of humans and mice with EoE, including R1 mice. However, direct evidence of T cell activation *in situ* in the esophagus is lacking, and most T cells recovered from human EoE biopsies are IFNγ-producing CD8 T

cells (12, 13, 16, 76). We propose that accumulation of T cells is a relatively late feature of EoE that reflects chronic inflammation initiated by innate cells. Lymphocyte-deficient R1 mice developed clinical and histologic features of EoE, and data from mouse models of other type 2 diseases corroborate that epithelial hyperplasia and eosinophil accumulation can occur in the absence of T cells (64, 77–79). Numerous chemokines expressed by R1 esophageal stromal cells are chemotactic for previously activated T cells and eosinophils (39, 80), providing a potential explanation for why food specific peTH2 cells in peripheral blood of patients with EoE would home to the esophagus as a consequence of epithelial dysfunction (13).

Growing evidence suggests that T cells are not the only, or even primary, source of Th2 cytokines in EoE. Tissue resident innate immune cells respond to alarmins released by distressed epithelial and stromal cells by producing type 2 cytokines. IL-33R^{high} mast cells and ILC2s concentrated at barrier surfaces are poised to quickly secrete type 2 cytokines in response to epithelial-derived alarmins, and both lineages are increased in human EoE biopsies (15, 68) and R1 esophagi. IL-13 from ILC2s drives smooth muscle proliferation and chemokine expression by fibroblasts (59). In patients with active EoE, activated mast cells express *IL5 and IL13* (51). IL-5 from activated ILC2s, mAPCs, and mast cells can support eosinophil proliferation and survival (59, 65). Once in a tissue, eosinophils themselves can perpetuate type 2 responses via expression of IL-4, IL-5, IL-9, IL-13 (42, 81).

We view the esophageal stroma as a dynamic innate immune tissue. Our work underscores the inherent potential for epithelium to control localized immune responses, and places TGFβ as a central regulator in this process. However, many questions remain. Redundancy, timing, and dose pose significant challenges to EoE treatment. Numerous cytokines, chemokines, and DAMPs are increased in the esophagi of individuals with EoE. Redundancy may explain why biologics targeting a single cytokine or receptor have been largely unsuccessful (82). Additionally, because different mediators act at different phases of allergic inflammation, the most efficacious therapeutic strategy will likely depend on the stage of disease progression when treatment is given. Finally, gene dosage appears to impact EoE pathogenesis. Most of the gene variants classified as EoE risk loci occur in non-coding regions of the gene, suggesting that changes in expression level contribute to EoE pathology. The R1 variant is a partial loss of signaling downstream of TGFβR. Other genetic models targeting TGFβ also found that dose matters. Haploinsufficiency of *Tgfb1* results in allergy, while complete loss results in autoimmunity (83). Overexpression of TGFβ in skin suppresses epidermal proliferation so completely that it is fatal (84). People homozygous for the *C509T* variant in *TGFB1* have an increased risk of developing EoE with features of EoEe3 (24). Thus, successful therapy for EoE will require identifying the correct targets, at the right time, and the ability to restore gene expression to physiological levels.

Overall, our findings place epithelium as a cornerstone of the allergic diathesis and expand the multi-dimensional role of TGFβ in maintaining immune homeostasis. A limitation of our study is that we focus on the role of epithelial cells as instigators of EoE. Additional studies will be required to determine whether or how other stromal cell and/or hematopoietic cell lineages contribute to EoE (14, 85–87). Further studies are also needed to understand

how external factors, such as microbiome and diet, influence epithelial homeostasis in the esophagus. We expect that mechanistic insight into the underlying etiology of eosinophilic inflammation in the esophagus is also highly relevant to other allergic conditions that occur in tissues lined by specialized epithelium, including atopic dermatitis, food allergy, and seasonal allergies (19, 88).

MATERIALS AND METHODS

Study Design

Individuals heterozygous for variants in *TGFBR1* are predisposed to develop allergic disease. The aim of this study is to identify the mechanisms responsible. We utilize mice with the $Tgfbr1^{M318R}$ variant knocked into the endogenous *Tgfbr1* locus and eosinophilic esophagitis (EoE) as a model of tissue restricted allergic inflammation. Flow cytometry, RNASeq, histology, immunohistochemistry, Western blots, ELISA, transmission electron microscopy, and epithelial barrier function assays are used to characterize the immunological, transcriptional, histological, and clinical features of disease that occur *in vivo*. Wild type age and sex matched cage mates serve as controls. *In vitro* organoid cultures are used to identify phenotypes that are epithelial cell intrinsic and occur spontaneously in the absence of external stimuli or other cell lineages. All data points and N values reflect biological replicates.

Animals

$Tgfbr1^{M318R}$ and $Tgfbr2^{G357W}$ knock-in mice were generated as previously described [4]. Homozygousity $Tgfbr1^{M318R/M318R}$ is embryonic lethal due to vascular malformations. Heterozygous $Tgfbr1^{M318R/+}$ (R1) mice were compared to age- and sex-matched controls homozygous for $Tgfbr1^{+/+}$. Heterozygous $Tgfbr2^{G357W}$ (R2) mice were compared to age- and sex-matched controls homozygous for $Tgfbr2^{+/+}$. R1 and WT mice were cohoused to minimize cage effects. Recombination Activating Gene 2 (RAG2) deficient mice were obtained from Taconic Farms. CD45.1 congenic mice were purchased from Jackson and backcrossed >12 generations with 129SvE mice purchased from Taconic Farms. IL-5 transgenic mice [132] and were bred onsite and housed under specific pathogen free conditions. Animals were maintained on a fixed diet of autoclaved water and chow (NIH-31M). All experiments were approved by the NIAID's ACUC and conducted in accordance with Animal Study Protocol (ASP) LAD11E. Gross photos were taken with a Canon PowerShot ELPH170 IS digital camera with 12X optical zoom.

Bone marrow chimeras

Adult and neonatal chimeras were generated as described (89).

Histology and immunohistochemistry (IHC)

Esophagi were fixed overnight in 1X phosphate buffered saline (1X PBS) with 4% Paraformaldehyde (PFA) (Electron Microscopy Sciences, Hatfield, PA) and then rinsed with 1X PBS. Fixed esophagi were cut in to 6 cross-sections, placed in 3% agarose, and then stored in 1X PBS. Paraffin embedding, sectioning, Hematoxylin and Eosin (H&E), staining was performed by HistoServ Inc. (Germantown, MD). Histochemical stains

were performed for collagen fibers (Masson's Trichrome) and mast cells and eosinophils (combined eosinophil-mast cell kit; American Mastertech, Lodi, CA). Immunohistochemical stains were used to identify eosinophils (Polyclonal goat anti-eosinophil major basic protein (EMBP1) (SantaCruz, Dallas TX sc-33938), and polyclonal rabbit anti-mouse CK6A (Biolegend, San Diego CA, 905701), polyclonal rabbit anti-mouse CK14 (Biolegend, San Diego CA, PRB-155p), rat anti-mouse S100A9 (Abcam, ab105472).

IHC staining was carried out on the Bond RX (Leica Biosystems) platform according to manufacturer-supplied protocols. Briefly, 5μm- thick sections were deparaffinized and rehydrated. Heat-induced epitope retrieval was performed using Epitope Retrieval Solution 1, pH 6.0, heated to 100° C for 20 min. The specimen was then incubated with hydrogen peroxide to quench endogenous peroxidase activity prior to applying the primary antibody. Detection with DAB chromogen was completed using the Bond Polymer Refine Detection kit (Leica Biosystems CAT# DS9800). Slides were finally cleared through gradient alcohol and xylene washes prior to mounting and coverslipping. Sections were examined by a board-certified veterinary pathologist using an Olympus BX51 light microscope and photomicrographs were taken using an Olympus DP73 camera.

Bromodeoxyuridine (BrdU)

Mice were injected intraperitoneally with BrdU (Sigma) in 1X PBS and then supplied with BrdU supplemented water for 24 hours. Esophagi and stomach were removed, fixed overnight in 1X PBS with 4 % PFA (Electron Microscopy Sciences), and then rinsed with 1X PBS. Paraffin embedding, sectioning, and immunohistochemical staining for BrdU was performed by HistoServ Inc. (Germantown, MD).

Transmission electron microscopy

4–6 pieces of tissue from the mid-esophagus of 8–12 wk old WT and R1 mice were fixed in 2.5 % glutaraldehyde/ 4 % PFA in 0.1 M phosphate buffer, washed three times with 0.1 M sodium cacodylate buffer and post fixed with 0.8 % $K_4Fe(CN)_6$/0.5 % OsO_4 in 0.1 M sodium cacodylate for 1 h. After three buffer washes, tissues were stained 1 h with 1 % tannic acid, and washed three times with dH_2O. Tissues were stained overnight with 1 % uranyl acetate, washed three times with dH_2O, and dehydrated with a graded ethanol series through 100 % ethanol and then twice with 100 % propylene oxide. Dehydrated tissues were infiltrated and embedded with epon/araldite resin and cured at 68° C. 80 nm sections were cut with a Leica UC6 ultramicrotome prior to viewing at 120 kV on a Tecnai BT Spirit transmission electron microscope (Thermo Fisher Scientific, formerly FEI). Digital images were acquired with an AMT digital camera system (AMT, Hazy, NY)

Intra-cellular space (ICS)

The mean intracellular distance between the cell bodies of adjacent basal cells was calculated by a blinded reviewer using Imaris software (version 9.7.2, Bitplane). Measurement Points tool was set to measure in pairs and used to measure distances between the cell bodies of adjacent basal cells in the whole image. Examples are shown in Fig S5. Statistical data were exported and mean intracellular space and standard deviation was calculated.

Cell isolations

Inflammatory cells from esophagi and stomachs—Esophagi were dissected, sliced open lengthwise, and rinsed in 1X PBS to remove ingesta. Each organ was placed in RPMI 1640 containing 0.1 mg/ml Liberase (Roche), 0.3 mg/ml DNAase I (Sigma), Penicillin/Streptomycin, and 10 mM HEPES, minced into small pieces, and then digested by incubating the tissue at 37° C for 15 min in an incubated shaker. The digestion reaction was stopped by the addition of cold RPMI supplemented with 10 % fetal bovine serum (FBS), 2 mM L-glutamine, 1 mM sodium pyruvate, 1X Non-essential amino acids, 1X Penicillin/Streptomycin (cRPMI). Digested tissue was sheered through an 18 G needle, filtered through 40 μM nylon mesh, and then washed with cRPMI.

Esophageal epithelial cells were isolated using a protocol adopted from (90). Briefly, esophagi were dissected, and the muscle layer manually removed. Inner esophagi were sliced open lengthwise and rinsed in 1X PBS to remove ingesta. Each organ was placed in 0.5 % Trypsin/EDTA (ThermoFisher), minced into small pieces, and then digested by incubating the tissue at 37° C for 20 min in an incubated shaker. The digestion reaction was stopped by the addition of cold keratinocyte serum free media supplemented with bovine pituitary extract and EGF (cKSFM) and trypsin inhibitor from soybeans (ThermoFisher). Digested tissue was filtered through 100 μM nylon mesh.

Intestinal Lamina Propria lymphocytes were isolated using a protocol adapted from Sheriden et al. (91). Briefly, small intestines were flushed with HBSS containing 10 mM HEPES and 5 % FBS and Peyer's Patches were removed. Small intestines and colons were cut longitudinally, remaining ingesta were removed, and then each organ was cut into small 2 mm^2 pieces. Intraepithelial lymphocytes were removed by 2 incubations in Hank's Balances Salt Solution (HBSS) with Dithiothreitol, HEPES & FBS. Epithelial cells were then removed by 2 incubations in HBSS with HEPES, L-glutamine, Penicillin/Streptomycin, and 1.3 mM EDTA. The remaining tissue was digested in RPMI with 100 U/ml collagenase I and then filtered through 70 μM nylon mesh. All incubations were all done in an incubated shaker at 37 °C. Single cells were resuspended in 44 % Percoll (Sigma), underlaid with 67.5 % Percoll, and then centrifuged at 2000 rpm for 20 min at 25° C. Cells were harvested from the 44 %/67.5 % interface and washed in RPMI 1640.

Spleen, lymph node, and thymus single cell suspensions of spleen and lymph node were made by crushing and filtering organs through 100 μM nylon mesh.

Bone Marrow cells were flushed from the femur and tibia of WT and R1 mice using a 26 G needle and 3 ml syringe and then filtered through 100 μM nylon mesh.

Peripheral Blood

For CBC peripheral blood was collected in EDTA tubes (Sarstedt) and analyzed by the PHL Hematology laboratory.

To isolate eosinophils for transwell assays: Whole blood samples from IL-5 transgenic mice were collected by retro-orbital bleeding into K3 EDTA coated tubes (Sarstedt). Blood was mixed immediately and vigorously to prevent clotting. Whole blood

was pooled up to 3 mice per tube, washed with cold 1X PBS containing 0.1 % BSA and 10 mM EDTA (PBS BSA EDTA) and passed through a 40 μM sterile filter. The blood was then centrifuged at 300 × g for 5 min at 4° C to pellet cells and the supernatant was aspirated. Red blood cells were lysed using distilled water followed by the addition of 10X PBS. The resulting cell pellet was resuspended in 100 μL of PBS BSA EDTA. Mouse anti-CD90.2, -CD45R/B220, and -Ly6B.2 MicroBeads (Miltenyi) were added to the cell suspension at a 20 μL per 1×10^7 cells. Cells were incubated in a rotating shaker for 15 min at 4° C. Cells were resuspended in 10 mL PBS BSA EDTA. Cells were added to an LD Column (Miltenyi) and allowed to elute. Unlabeled eosinophils in effluent were collected. Isolated eosinophils were counted and resuspended in chemotaxis media at a concentration of 1×10^6 cells/mL

Flow cytometry

Cells were analyzed on an LSR II Flow cytometer (BD Biosciences) or Aurora Spectral Flow cytometer (Cytek). Data were analyzed in FlowJo (Treestar). Viability was monitored by Live Dead Fixable (Invitrogen) or Zombie dyes (Biolegend). All samples were Fc-Blocked with purified anti-mouse CD16/32 prior to surface staining. Intracellular staining was performed using Lyse Fix solution and Perm Buffer III (BD Biosciences) according to the manufacturer' instructions. Antibodies and Brilliant Violet staining buffer were purchased from BD Biosciences, Biolegend, and eBioscience (Table S8). Hematopoietic cell lineages were identified by applying the following gating criteria to Live $CD45^+$ single cells: eosinophils ($CD11b^+SiglecF^+$), myeloid antigen presenting cells (mAPC) ($CD11b^+MHC2^+$), mast cells ($CD11b^{neg}Kit^+Fc\varepsilon R1^+$), ILC2s ($Lin^{neg+}ST2^+KLRG1^+Sca1^+$), T cells ($CD3\varepsilon^+$), B cells ($CD19^+$), basophils ($CD11b^{neg}MHC2^{neg}CD3\varepsilon^{neg}CD19^{neg}Kit^{neg}CD49b^+Fc\varepsilon R1^+$), granulocytes ($CD11b^+MHC2^{neg}GR1^+$), NK cells ($CD11b^{neg}MHC2^{neg}CD3\varepsilon^{neg}CD49b^+$). Epithelial cells were defined as Live $CD326^+$ $CD45^{neg}$ single cells. See also Fig. S2.

Hydroxyproline

The extent of fibrosis in the esophagus was determined by quantifying hydroxyproline levels as described in [10].

RNASeq

Esophagi from 16 week old WT and *Tgfbr1*$^{M318R/+}$ (R1) mice were harvested, muscle was manually removed, and the inner esophagi were snap frozen with liquid nitrogen and stored at -80°C until RNA isolation. Total RNA was isolated from the inner esophagi of individual WT (N=9) and R1 (N=9) mice (Direct-zol RNA miniprep Plus; Zymo Research Corp., Irvine CA). All samples had an RNA Integrity (RIN) number of >9.00. PolyA selected mRNA libraries were generated using the Illumina TruSeq Stranded Library protocol, and mRNA samples were pooled and sequenced on a HiSeq2500 (Frederick National Laboratory for Cancer Research, NIH). All the samples had a raw yield >=42 million paired-end 125 base-pair reads, and downstream bioinformatic analysis was conducted using the CCBR RNA-Seq pipeline (https://github.com/CCBR/Pipeliner). Both reads of each sample were trimmed for contaminating adapters and low-quality bases using Trimmomatic v0.36 (92) and aligned to the mouse *mm10* reference genome and Gencode vM9 annotation using STAR v2.5.3 (93). RSEM v1.3.0 (94) was used for gene-level expression quantification, and *voom* quantile normalization implemented in the R package limma v3.36.5 (95) was used

to generate normalized gene expression values. Only genes expressed at a level of 1 CPM across all 3 samples were carried forward for expression analysis. Read- and alignment-level quality was assessed using MultiQC v0.9 (http://multiqc.info/) to aggregate QC metrics from FastQC (http://www.bioinformatics.babraham.ac.uk/projects/fastqc/), FastQ Screen (https://www.bioinformatics.babraham.ac.uk/projects/fastq_screen/), Picard, RSeQC (http://rseqc.sourceforge.net/) and Trimmomatic. To compare our mouse model with the three recognized human endotypes, we obtained the mean expression values for each gene on the 96-gene EoE Diagnostic Panel (EDP) (6) for each of the three recognized endotypes. In heat maps, each lane is gene expression from an individual WT or R1 mouse.

Barrier function assays

Barrier function assays were performed using a Ussing Chamber (Physiological Instruments, San Diego CA). The distal half of esophagi were dissected, rinsed with cold Krebs-Carbonate buffer (KBR), and tissue was mounted in a P2406 slider (area 0.04 cm^2). Both sides of the chambers were filled with Krebs-Ringer Bicarbonate Buffer supplemented with 1.2 mM $CaCl_2$, 1.2 mM $MgCl_2$, and 10 mM glucose. Chambers were maintained at 37° C and continuously oxygenated and circulated by gas flow (95% O_2/5% CO_2).

Transepithelial electrical resistance (TEER)

Ag/Cl electrodes with KBR/2 % agar bridges were used to measure transepithelial potential difference (PD) and current (I). After equilibration for 30 min, basal electrical readings of potential difference (PD), short circuit current (Isc), and total electrical resistance (R_T) were recorded every 30 sec for 90 min using Acquire & Analyze software (Physiological Instruments). Data are the mean R_T of the middle 30 min in Kiloohms (KO)/cm^2.

Permeability

10 mg/ml of FITC-Dextran (FD4; Sigma, St. Louis, MO) and 10 mg/ml of Rhodamine B isothiocyanate-Dextran (R9379; Sigma, St. Louis MO) were added to the mucosal side of the chamber. The serosal side of the chambers was sampled every 30 min for a total of 3 h. The optical densities of the fluorescent tracers were determined using a Tecan-HP plate reader. Absolute values of each tracer were calculated from a standard curve. To determine the maximum diffusion, one chamber was left empty (E) without esophageal tissue.

Western Blotting

Lysates—Total esophagi were removed, and the inner (E) and outer (M) layers were separated from one another. A section of small intestine (SI) equivalent to the length of the esophagus was isolated from an R1 mouse. Each tissue was immediately placed in a 2.0 ml tube prefilled with 3 mm High Impact Zironium beads (Benchmark Scientific) and 0.5 ml cold RIPA buffer with protease/phosphatase inhibitors (ThermoFisher). Tissue was homogenized using a BeadBlaster homogenizer (MidSci; St. Louis, MO). After spinning at 10,000 g for 20 min the supernatant was transferred to a new tube and stored at -80° C until blotting.

Gels and Blotting—Samples were denatured by heating to 95° C for 10 min in a heat block and mixed with NuPAGE LDS sample buffer containing reducing agent (ThermoFisher). Samples were run in a NuPAGE Novex 4–12 % Bis-Tris gel with MES running buffer (ThermoFisher) and then proteins were transferred to polyvinylidene difluoride (PVDF) membranes using an iBlot (ThermoFisher). Membranes were blocked with 5 % Non-fat dry milk (NFDM) in 1X PBS supplemented with 0.1 % Tween 20 (PBST) at room temperature. Membranes were incubated overnight at 4° C with primary antibody diluted in 2.5 % NFDM. The next day membranes were washed with PBST and then incubated with secondary antibody diluted in 2.5 % NFDM. Even loading was monitored by stripping blots with Restore Plus Western Stripping Buffer (ThermoFisher) and reblotting.

Antibodies—Primary antibodies anti-mouse- S100A9, S100A8 (R&D), ECF/CHI3L3/4/Ym1/2 (AbCam), and Hsp90 (Cell Signaling). Horseradish peroxidase conjugated secondary antibodies were purchased from Jackson Immunoresearch and Cell Signaling. Secondary antibodies were visualized with SuperSignal West Dura or Pico substrate (Pierce) and imaged on a Biorad Chemidock Imager.

RT-PCR—Esophagus inner layers were collected from 8–10 wk old R1 and WT mice. Tissues were homogenized immediately, and total RNA was extracted using TRIzol Reagent (ThermoFisher Scientific, Carlsbad, CA). cDNA was made using iScript Reverse Transcription kit (BIO-RAD, Hercules, CA) according to the manufacturer's instruction. TaqMan probes (Applied Biosystems, Foster city, CA) (Table S9) were used to evaluate the gene expression level using quantitative polymerase chain reaction (qPCR). Glyceraldehyde 3-phosphate dehydrogenase (GAPDH) probe was used as an internal control. All PCR reactions were performed on BIO-RAD CFX96 real time machine. The threshold cycle (CT) values of the genes were determined for each sample. The genes that has CT value greater than 39 was considered undetectable. The fold-change in gene expression was calculated as $2\Delta\Delta CT$; where $\Delta\Delta CT = \Delta CT$ (R1 mouse) – ΔCT (WT mouse); $\Delta CT = (CT(gene) - CT(GAPDH)$. All samples were run in duplicate with $N \geq 12$ mice per group analyzed individually.

Organoid Cultures—Organoid culture conditions were adopted from (96, 97). Briefly, the inner epithelial layer was mechanically dissected from esophagi isolated from 8–10 wk old mice and incubated in complete chelating solution (CCS; 6 mM $Na_2HPO_4.H_2O$, 8 mM KH_2PO_4, 0.1M NaCl, 1.5 mM KCl, 40 mM sucrose, 60mM D-sorbital, 1 mM DTT) for 15 min then manually minced. CCS was removed by centrifugation at 400 g for 10 min at 4°C, and pellet was then incubated in 1X Trypsin-EDTA at 37°C for 60 min, vortexing every 15 min. Trypsin was inactivated with DMEM+12 % FBS and the suspension was passed through a 70 μm sterile filter. Media was removed by centrifugation and cells were suspended in Matrigel® (Corning) then placed in a 24-well tissue culture plate and polymerized at 37°C for 20 min. Media (Advanced DMEM/F-12 supplemented with 10 mM HEPES, 1% GlutaMAX, 1% penicillin-streptomycin, 100 μg/ml Primocin, 50 ng/ml EGF (Biotechne), 2% B27 Supplement, 1mM N-Acetylcysteine (Sigma), 50% Wnt3A-conditioned medium (L Wnt3A from ATCC, CRL-2647), 15% R-Spondin 1-conditioned medium (HEK293T cells stably expressing mouse Rspo1-Fc from Dr. Calvin Kuo, Stanford

University),10% Noggin-conditioned medium (HEK293T cells stably expressing murine Noggin-Fc from Dr. Gijs R. van den Brink, Tytgat Institute for Liver and Intestinal Research and Department of Gastroenterology and Hepatology, Academic Medical Center, Amsterdam, The Netherlands)) was added to cover Matrigel and changed every 48 h for 14 days. Unless otherwise indicated, media components were from ThermoFisher Scientific.

EdU proliferation assay—Organoids were grown for 14 d and then stained using the Click-iT™ EdU Cell Proliferation Kit for Imaging, AlexaFluor™488 dye (ThermoFisher) following manufacturer's instructions with the following modifications: concentration of EdU was increased to 50 μm for labeling, incubation time with EdU was 3 h, incubation time for cell fixation and permeabilization was 1 h. Images of enteroids, N=34 WT and N=36 R1, were obtained with an Olympus FV3000RS confocal microscope focused in the equatorial plane of each organoid. Using MetaMorph 7.8.8 (Molecular Devices, Downingtown, PA) the outer rim of cells in the equatorial plane was isolated with a mask containing the outer perimeter extending inward 10 pixels to exclude out of plane cells. The number of pixels above threshold was calculated separately for AlexaFluor488 and Hoechst 33342.

Luminex magnetic bead assay—Assay was performed as per Manufacturer's instructions (R&D Systems) using WT and R1 organoid conditioned media. Plates were read using a Millipore MAGPIX System (Millipore Sigma).

Chemotaxis assay—Chemotaxis assay was performed using an AP48 Neuro Probe Multiwell Chamber with an 8.0 μm filter pore size. Chemotaxis media was prepared using RPMI 1640, 1.0% FBS, and 10 mM HEPES. 5.6×10^4 isolated peripheral blood eosinophils from IL-5 transgenic mice were added to the top chamber. Organoid base media was added to the bottom chamber and served as a vehicle control. WT and R1 conditioned media were added to the bottom chamber and served as the sample analytes. The chamber was incubated at 37° C for 2 h in 5% CO_2 to allow for transmigration between the wells. After 2 h, the number of migrated eosinophils in the lower chamber was determined. Eosinophils were identified by their forward and side scatter properties on the BD LSRII flow cytometer and analyzed on FlowJo software. Chemotactic index was calculated as the number of eosinophils migrated to conditioned media/number of eosinophils migrated to unconditioned media.

Statistics

Data were analyzed by non-parametric non-paired two-tailed Mann-Whitney U statistical tests using with GraphPad Prism 7.00 for Windows, (GraphPad Software, La Jolla CA). Data are expressed as mean ± SEM. Differences were considered significant (*) when $P < 0.05$ and non-significant (n.s.) when $P > 0.05$. The number of biological replicates (N) and statistical tests performed were based upon previous experience and in consultation with statisticians in NIAID's Bioinformatics Services Branch (NIAID, NIH). For gene expression analysis, sample sizes were determined based upon recommendations of staff of the Frederick National Laboratory for Cancer Research Sequencing Core Facility (NCI, NIH). Differences were considered significant when false discovery rate (FDR) <0.10.

Supplementary Material

Refer to Web version on PubMed Central for supplementary material.

Acknowledgments:

The authors would like to acknowledge Andrew Hirsch (Physiologic Instruments) for expert assistance with Ussing Chamber experiments, Jingwen Gu (NIAID Bioinformatics Services) for statistical analyses, Dana Scott (NIAID) for assistance with the interpretation of TEM images, George McNamara for help with image processing of confocal images, Research Support Specialists Philip Dugan and Lashawna Leak (NIAID Comparative Medicine Branch) for assistance with animal work, David Stephany (NIAID Flow Cytometry Core) for assistance with MAGPIX, Mahnaz Minai (NIAID) for IHC, Helene Rosenberg for expert advice on eosinophil transmigration experiments, mentorship and support of A.R.L., and review of the manuscript, and Josh Milner and Yasmine Belkaid for critical review of the manuscript. We also acknowledge the National Institute of Diabetes and Digestive and Kidney Diseases-funded Integrated Physiology Core of the Johns Hopkins Conte Digestive Disease Basic and Translational Research Core Center for establishing organoid cultures and providing growth factor conditioned media.

Funding:

This research was supported by Intramural Research Program of the National Institute of Allergy and Infectious Diseases (ZAI001203-01; P.F.-G.); (ZAI000941; H.R.), (ZAI000829, ZAI001019; T.W.); Loeys-Dietz Syndrome Foundation (P.F.-G., A.L.G., H.C.D.); Food Allergy Research and Education Foundation (FARE; P.F-G.); NIH K23 Mentored Research Development Award (K23AI091869; P.F.-G.); ARTrust Faculty Development Award (P.F.-G.) Johns Hopkins University Clinician Scientist Award (P.F.-G.); Johns Hopkins Conte Digestive Diseases Basic and Translational Research Core Grant (P.F.-G.); George Ferry Young Investigator Development Award (North American Society for Pediatric Gastroenterology Hepatology and Nutrition (A.L.G.); NIH K08 Mentored Research Development Award (1K08DK106463; A.L.G.); NIH P30-DK089502 (N.Z., R.L.); NIH R01- AR41135-18 (H.C.D.); HHMI (H.C.D.) William S. Smilow Center for Marfan Syndrome Research (H.C.D.); NIH shared instrumentation grant (1S10OD025244-01; A.L.G.).

Data and materials availability:

RNASeq data have been deposited into the Geo Repository Accession number GSE193756. All data needed to evaluate the conclusions in this paper are present in the paper or the Supplementary Materials.

REFERENCES

1. Davis BP, Rothenberg ME, Mechanisms of Disease of Eosinophilic Esophagitis. Annu Rev Pathol 11, 365–393 (2016). [PubMed: 26925500]
2. Frischmeyer-Guerrerio PA, Guerrerio AL, Oswald G, Chichester K, Myers L, Halushka MK, Oliva-Hemker M, Wood RA, Dietz HC, TGFbeta receptor mutations impose a strong predisposition for human allergic disease. Sci Transl Med 5, 195ra194 (2013).
3. Gallo EM, Loch DC, Habashi JP, Calderon JF, Chen Y et al. , Angiotensin II-dependent TGF-beta signaling contributes to Loeys-Dietz syndrome vascular pathogenesis. J Clin Invest 124, 448–460 (2014). [PubMed: 24355923]
4. Cardoso S, Robertson SP, Daniel PB, TGFBR1 mutations associated with Loeys-Dietz syndrome are inactivating. J Recept Signal Transduct Res 32, 150–155 (2012). [PubMed: 22414221]
5. Collins MH, Martin LJ, Alexander ES, Boyd JT, Sheridan R et al. , Newly developed and validated eosinophilic esophagitis histology scoring system and evidence that it outperforms peak eosinophil count for disease diagnosis and monitoring. Dis Esophagus 30, 1–8 (2017).
6. Wen T, Stucke EM, Grotjan TM, Kemme KA, Abonia JP et al. , Molecular diagnosis of eosinophilic esophagitis by gene expression profiling. Gastroenterology 145, 1289–1299 (2013). [PubMed: 23978633]

7. Shoda T, Wen T, Aceves SS, Abonia JP, Atkins D et al. , Eosinophilic oesophagitis endotype classification by molecular, clinical, and histopathological analyses: a cross-sectional study. Lancet Gastroenterol Hepatol 3, 477–488 (2018). [PubMed: 29730081]
8. Verrecchia F, Chu ML, Mauviel A, Identification of novel TGF-beta /Smad gene targets in dermal fibroblasts using a combined cDNA microarray/promoter transactivation approach. J Biol Chem 276, 17058–17062 (2001). [PubMed: 11279127]
9. Wynn TA, Barron L, Thompson RW, Madala SK, Wilson MS, Cheever AW, Ramalingam T, Quantitative assessment of macrophage functions in repair and fibrosis. Curr Protoc Immunol Chapter 14, Unit14 22 (2011).
10. Blanchard C, Wang N, Stringer KF, Mishra A, Fulkerson PC et al. , Eotaxin-3 and a uniquely conserved gene-expression profile in eosinophilic esophagitis. J Clin Invest 116, 536–547 (2006). [PubMed: 16453027]
11. Sherrill JD, Kiran KC, Blanchard C, Stucke EM, Kemme KA et al. , Analysis and expansion of the eosinophilic esophagitis transcriptome by RNA sequencing. Genes Immun 15, 361–369 (2014). [PubMed: 24920534]
12. Wen T, Aronow BJ, Rochman Y, Rochman M, Kc K et al. , Single-cell RNA sequencing identifies inflammatory tissue T cells in eosinophilic esophagitis. J Clin Invest 130, 2014–2028 (2019).
13. Morgan DM, Ruiter B, Smith NP, Tu AA, Monian B et al. , Clonally expanded, GPR15-expressing pathogenic effector TH2 cells are associated with eosinophilic esophagitis. Sci Immunol 6, eabi5586 (2021). [PubMed: 34389613]
14. Aceves SS, Chen D, Newbury RO, Dohil R, Bastian JF, Broide DH, Mast cells infiltrate the esophageal smooth muscle in patients with eosinophilic esophagitis, express TGF-beta1, and increase esophageal smooth muscle contraction. J Allergy Clin Immunol 126, 1198–1204 (2010). [PubMed: 21047675]
15. Doherty TA, Baum R, Newbury RO, Yang T, Dohil R et al. , Group 2 innate lymphocytes (ILC2) are enriched in active eosinophilic esophagitis. J Allergy Clin Immunol 136, 792–794 (2015). [PubMed: 26233928]
16. Lucendo AJ, Navarro M, Comas C, Pascual JM, Burgos E, Santamaria L, Larrauri J, Immunophenotypic characterization and quantification of the epithelial inflammatory infiltrate in eosinophilic esophagitis through stereology: an analysis of the cellular mechanisms of the disease and the immunologic capacity of the esophagus. Am J Surg Pathol 31, 598–606 (2007). [PubMed: 17414108]
17. Shull MM, Ormsby I, Kier AB, Pawlowski S, Diebold RJ et al. , Targeted disruption of the mouse transforming growth factor-beta 1 gene results in multifocal inflammatory disease. Nature 359, 693–699 (1992). [PubMed: 1436033]
18. Dellon ES, Liacouras CA, Molina-Infante J, Furuta GT, Spergel JM et al. , Updated International Consensus Diagnostic Criteria for Eosinophilic Esophagitis: Proceedings of the AGREE Conference. Gastroenterology 155, 1022–1033 (2018). [PubMed: 30009819]
19. Goleva E, Berdyshev E, Leung DY, Epithelial barrier repair and prevention of allergy. J Clin Invest 129, 1463–1474 (2019). [PubMed: 30776025]
20. Streubel MK, Rinnerthaler M, Bischof J, Richter K, Changes in the Composition of the Cornified Envelope During Skin Aging: A Calcium Centric Point of View. Farage MA, Miller KW, Maibach HI, Eds., Textbook of aging skin (Springer, Berlin, ed. 1, 2010), pp. xxxv, 1220 p.
21. Capocelli KE, Fernando SD, Menard-Katcher C, Furuta GT, Masterson JC, Wartchow EP, Ultrastructural features of eosinophilic oesophagitis: impact of treatment on desmosomes. J Clin Pathol 68, 51–56 (2015). [PubMed: 25359789]
22. Jensen PJ, Telegan B, Lavker RM, Wheelock MJ, E-cadherin and P-cadherin have partially redundant roles in human epidermal stratification. Cell Tissue Res 288, 307–316 (1997). [PubMed: 9082966]
23. Rochman M, Travers J, Miracle CE, Bedard MC, Wen T et al. , Profound loss of esophageal tissue differentiation in patients with eosinophilic esophagitis. J Allergy Clin Immunol 140, 738–749 (2017). [PubMed: 28104354]

24. Rawson R, Yang T, Newbury RO, Aquino M, Doshi A et al. , TGF-beta1-induced PAI-1 contributes to a profibrotic network in patients with eosinophilic esophagitis. J Allergy Clin Immunol 138, 791–800 e794 (2016). [PubMed: 27212082]
25. Finnegan A, Cho RJ, Luu A, Harirchian P, Lee J, Cheng JB, Song JS, Single-Cell Transcriptomics Reveals Spatial and Temporal Turnover of Keratinocyte Differentiation Regulators. Front Genet 10, 775 (2019). [PubMed: 31552090]
26. Nagarajan P, Chin SS, Wang D, Liu S, Sinha S, Garrett-Sinha LA, Ets1 blocks terminal differentiation of keratinocytes and induces expression of matrix metalloproteases and innate immune mediators. J Cell Sci 123, 3566–3575 (2010). [PubMed: 20930145]
27. Stoner GD, Kaighn ME, Reddel RR, Resau JH, Bowman D et al. , Establishment and characterization of SV40 T-antigen immortalized human esophageal epithelial cells. Cancer Res 51, 365–371 (1991). [PubMed: 1703038]
28. Massague J, Gomis RR, The logic of TGFbeta signaling. FEBS Lett 580, 2811–2820 (2006). [PubMed: 16678165]
29. Zhang Y, Alexander PB, Wang XF, TGF-beta Family Signaling in the Control of Cell Proliferation and Survival. Cold Spring Harb Perspect Biol 9, a022145 (2017). [PubMed: 27920038]
30. Pietenpol JA, Holt JT, Stein RW, Moses HL, Transforming growth factor beta 1 suppression of c-myc gene transcription: role in inhibition of keratinocyte proliferation. Proc Natl Acad Sci USA 87, 3758–3762 (1990). [PubMed: 2187192]
31. Aceves SS, Newbury RO, Dohil R, Schwimmer J, Bastian JF, Distinguishing eosinophilic esophagitis in pediatric patients: clinical, endoscopic, and histologic features of an emerging disorder. J Clin Gastroenterol 41, 252–256 (2007). [PubMed: 17426462]
32. Yano S, Banno T, Walsh R, Blumenberg M, Transcriptional responses of human epidermal keratinocytes to cytokine interleukin-1. J Cell Physiol 214, 1–13 (2008). [PubMed: 17941080]
33. Juráňová J FJ, Ulrichová J, The role of keratinocytes in inflammation. J Appl Biomed. 15, 169–179 (2017).
34. Bando M, Hiroshima Y, Kataoka M, Shinohara Y, Herzberg MC, Ross KF, Nagata T, Kido J, Interleukin-1α regulates antimicrobial peptide expression in human keratinocytes. Immunol Cell Biol 85, 532–537 (2007). [PubMed: 17549071]
35. Banno T, Gazel A, Blumenberg M, Effects of tumor necrosis factor-alpha in epidermal keratinocytes revealed using global transcriptional profiling. J Biol Chem 279, 32633–32642 (2004). [PubMed: 15145954]
36. Haider AS, Lowes MA, Suarez-Farinas M, Zaba LC, Cardinale I, Blumenberg M, Krueger JG, Cellular genomic maps help dissect pathology in human skin disease. J Invest Dermatol 128, 606–615 (2008). [PubMed: 17928892]
37. Komine M, Rao LS, Freedberg IM, Simon M, Milisavljevic V, Blumenberg M, Interleukin-1 induces transcription of keratin K6 in human epidermal keratinocytes. J Invest Dermatol 116, 330–338 (2001). [PubMed: 11180011]
38. Freedberg IM, Tomic-Canic M, Komine M, Blumenberg M, Keratins and the keratinocyte activation cycle. J Invest Dermatol 116, 633–640 (2001). [PubMed: 11348449]
39. Yoshie O, Matsushima K, CCR4 and its ligands: from bench to bedside. Int Immunol 27, 11–20 (2015). [PubMed: 25087232]
40. Viney JM, Andrew DP, Phillips RM, Meiser A, Patel P et al. , Distinct conformations of the chemokine receptor CCR4 with implications for its targeting in allergy. J Immunol 192, 3419–3427 (2014). [PubMed: 24563252]
41. Nagata M, Nakagome K, Soma T, Mechanisms of eosinophilic inflammation. Asia Pac Allergy 10, e14 (2020). [PubMed: 32411579]
42. Lampinen M, Carlson M, Hakansson LD, Venge P, Cytokine-regulated accumulation of eosinophils in inflammatory disease. Allergy 59, 793–805 (2004). [PubMed: 15230810]
43. Gonlugur U, Efeoglu T, Vascular adhesion and transendothelial migration of eosinophil leukocytes. Cell Tissue Res 318, 473–482 (2004). [PubMed: 15578268]
44. Gong T, Liu L, Jiang W, Zhou R, DAMP-sensing receptors in sterile inflammation and inflammatory diseases. Nat Rev Immunol 20, 95–112 (2020). [PubMed: 31558839]

45. Plager DA, Torres SM, Koch SN, Kita H, Gene transcription abnormalities in canine atopic dermatitis and related human eosinophilic allergic diseases. Vet Immunol Immunopathol 149, 136–142 (2012). [PubMed: 22749291]
46. Hayashi N, Kido J, Kido R, Wada C, Kataoka M, Shinohara Y, Nagata T, Regulation of calprotectin expression by interleukin-1alpha and transforming growth factor-beta in human gingival keratinocytes. J Periodontal Res 42, 1–7 (2007). [PubMed: 17214633]
47. Wang S, Song R, Wang Z, Jing Z, Wang S, Ma J, S100A8/A9 in Inflammation. Front Immunol 9, 1298 (2018). [PubMed: 29942307]
48. Owhashi M, Arita H, Hayai N, Identification of a novel eosinophil chemotactic cytokine (ECF-L) as a chitinase family protein. J Biol Chem 275, 1279–1286 (2000). [PubMed: 10625674]
49. Nio J, Fujimoto W, Konno A, Kon Y, Owhashi M, Iwanaga T, Cellular expression of murine Ym1 and Ym2, chitinase family proteins, as revealed by in situ hybridization and immunohistochemistry. Histochem Cell Biol 121, 473–482 (2004). [PubMed: 15148607]
50. Chang M, McNinch J, Elias C 3rd, Manthey CL, Grosshans D, Meng T, Boone T, Andrew DP, Molecular cloning and functional characterization of a novel CC chemokine, stimulated T cell chemotactic protein (STCP-1) that specifically acts on activated T lymphocytes. J Biol Chem 272, 25229–25237 (1997). [PubMed: 9312138]
51. Ben-Baruch Morgenstern N, Ballaban AY, Wen T, Shoda T, Caldwell JM et al. , Single-cell RNA sequencing of mast cells in eosinophilic esophagitis reveals heterogeneity, local proliferation, and activation that persists in remission. J Allergy Clin Immunol 149, 2062–2077 (2022). [PubMed: 35304158]
52. DiScipio RG, Daffern PJ, Jagels MA, Broide DH, Sriramarao P, A comparison of C3a and C5a-mediated stable adhesion of rolling eosinophils in postcapillary venules and transendothelial migration in vitro and in vivo. J Immunol 162, 1127–1136 (1999). [PubMed: 9916743]
53. Erger RA, Casale TB, Tumor necrosis factor alpha is necessary for granulocyte-macrophage-colony-stimulating-factor-induced eosinophil transendothelial migration. Int Arch Allergy Immunol 115, 24–32 (1998). [PubMed: 9430492]
54. Nickoloff BJ, Turka LA, Keratinocytes: key immunocytes of the integument. Am J Pathol 143, 325–331 (1993). [PubMed: 8342589]
55. Jiang Y, Tsoi LC, Billi AC, Ward NL, Harms PW, Zeng C, Maverakis E, Kahlenberg JM, Gudjonsson JE, Cytokinocytes: the diverse contribution of keratinocytes to immune responses in skin. JCI Insight 5, e142067 (2020). [PubMed: 33055429]
56. Cao W, Cheng L, Behar J, Fiocchi C, Biancani P, Harnett KM, Proinflammatory cytokines alter/reduce esophageal circular muscle contraction in experimental cat esophagitis. Am J Physiol Gastrointest Liver Physiol 287, G1131–1139 (2004). [PubMed: 15271650]
57. Patel S, Danger-Associated Molecular Patterns (DAMPs): the Derivatives and Triggers of Inflammation. Curr Allergy Asthma Rep 18, 63 (2018). [PubMed: 30267163]
58. Gieseck RL 3rd, Wilson MS, Wynn TA, Type 2 immunity in tissue repair and fibrosis. Nat Rev Immunol 18, 62–76 (2018). [PubMed: 28853443]
59. Choi HS, Won T, Hou X, Chen G, Bracamonte-Baran W et al. , Innate Lymphoid Cells Play a Pathogenic Role in Pericarditis. Cell Rep 30, 2989–3003 (2020). [PubMed: 32130902]
60. Loh Z, Simpson J, Ullah A, Zhang V, Gan WJ et al. , HMGB1 amplifies ILC2-induced type-2 inflammation and airway smooth muscle remodelling. PLoS Pathog 16, e1008651 (2020). [PubMed: 32658914]
61. Ohne Y, Silver JS, Thompson-Snipes L, Collet MA, Blanck JP, Cantarel BL, Copenhaver AM, Humbles AA, Liu YJ, IL-1 is a critical regulator of group 2 innate lymphoid cell function and plasticity. Nat Immunol 17, 646–655 (2016). [PubMed: 27111142]
62. Ptaschinski C, Rasky AJ, Fonseca W, Lukacs NW, Stem Cell Factor Neutralization Protects From Severe Anaphylaxis in a Murine Model of Food Allergy. Front Immunol 12, 604192 (2021). [PubMed: 33786039]
63. Eiwegger T, Akdis CA, IL-33 links tissue cells, dendritic cells and Th2 cell development in a mouse model of asthma. Eur J Immunol 41, 1535–1538 (2011). [PubMed: 21618506]
64. Kondo Y, Yoshimoto T, Yasuda K, Futatsugi-Yumikura S, Morimoto M, Hayashi N, Hoshino T, Fujimoto J, Nakanishi K, Administration of IL-33 induces airway hyperresponsiveness and goblet

cell hyperplasia in the lungs in the absence of adaptive immune system. Int Immunol 20, 791–800 (2008). [PubMed: 18448455]

65. Yang Z, Grinchuk V, Urban JF Jr., Bohl J, Sun R et al. , Macrophages as IL-25/IL-33-responsive cells play an important role in the induction of type 2 immunity. PLoS One 8, e59441 (2013). [PubMed: 23536877]
66. Nelson M, Zhang X, Pan Z, Spechler SJ, Souza RF, Mast cell effects on esophageal smooth muscle and their potential role in eosinophilic esophagitis and achalasia. Am J Physiol Gastrointest Liver Physiol 320, G319–G327 (2021). [PubMed: 33355505]
67. Zhang Z, Kurashima Y, Two Sides of the Coin: Mast Cells as a Key Regulator of Allergy and Acute/Chronic Inflammation. Cells 10, (2021).
68. Bolton SM, Kagalwalla AF, Arva NC, Wang MY, Amsden K et al. , Mast Cell Infiltration Is Associated With Persistent Symptoms and Endoscopic Abnormalities Despite Resolution of Eosinophilia in Pediatric Eosinophilic Esophagitis. Am J Gastroenterol 115, 224–233 (2020). [PubMed: 31913192]
69. Akei HS, Mishra A, Blanchard C, Rothenberg ME, Epicutaneous antigen exposure primes for experimental eosinophilic esophagitis in mice. Gastroenterology 129, 985–994 (2005). [PubMed: 16143136]
70. Mishra A, Hogan SP, Brandt EB, Rothenberg ME, An etiological role for aeroallergens and eosinophils in experimental esophagitis. J Clin Invest 107, 83–90 (2001). [PubMed: 11134183]
71. Rubinstein E, Cho JY, Rosenthal P, Chao J, Miller M, Pham A, Aceves SS, Varki A, Broide DH, Siglec-F inhibition reduces esophageal eosinophilia and angiogenesis in a mouse model of eosinophilic esophagitis. J Pediatr Gastroenterol Nutr 53, 409–416 (2011). [PubMed: 21970996]
72. Hogan SP, Mishra A, Brandt EB, Royalty MP, Pope SM, Zimmermann N, Foster PS, Rothenberg ME, A pathological function for eotaxin and eosinophils in eosinophilic gastrointestinal inflammation. Nat Immunol 2, 353–360 (2001). [PubMed: 11276207]
73. Inage E, Furuta GT, Menard-Katcher C, Masterson JC, Eosinophilic esophagitis: pathophysiology and its clinical implications. Am J Physiol Gastrointest Liver Physiol 315, G879–G886 (2018). [PubMed: 30212252]
74. Blanchard C, Stucke EM, Burwinkel K, Caldwell JM, Collins MH et al. , Coordinate interaction between IL-13 and epithelial differentiation cluster genes in eosinophilic esophagitis. J Immunol 184, 4033–4041 (2010). [PubMed: 20208004]
75. Rochman M, Xie YM, Mack L, Caldwell JM, Klingler AM, Osswald GA, Azouz NP, Rothenberg ME, Broad transcriptional response of the human esophageal epithelium to proton pump inhibitors. J Allergy Clin Immunol 147, 1924–1935 (2021). [PubMed: 33289661]
76. Ruffner MA, Hu A, Dilollo J, Benocek K, Shows D et al. , Conserved IFN Signature between Adult and Pediatric Eosinophilic Esophagitis. J Immunol 206, 1361–1371 (2021). [PubMed: 33558373]
77. Yoo J, Omori M, Gyarmati D, Zhou B, Aye T, Brewer A, Comeau MR, Campbell DJ, Ziegler SF, Spontaneous atopic dermatitis in mice expressing an inducible thymic stromal lymphopoietin transgene specifically in the skin. J Exp Med 202, 541–549 (2005). [PubMed: 16103410]
78. Salimi M, Barlow JL, Saunders SP, Xue L, Gutowska-Owsiak D et al. , A role for IL-25 and IL-33-driven type-2 innate lymphoid cells in atopic dermatitis. J Exp Med 210, 2939–2950 (2013). [PubMed: 24323357]
79. Boberg E, Johansson K, Malmhall C, Calven J, Weidner J, Radinger M, Interplay Between the IL-33/ST2 Axis and Bone Marrow ILC2s in Protease Allergen-Induced IL-5-Dependent Eosinophilia. Front Immunol 11, 1058 (2020). [PubMed: 32582171]
80. Vestergaard C, Bang K, Gesser B, Yoneyama H, Matsushima K, Larsen CG, A Th2 chemokine, TARC, produced by keratinocytes may recruit CLA+CCR4+ lymphocytes into lesional atopic dermatitis skin. J Invest Dermatol 115, 640–646 (2000). [PubMed: 10998136]
81. Valent P, Degenfeld-Schonburg L, Sadovnik I, Horny HP, Arock M, Simon HU, Reiter A, Bochner BS, Eosinophils and eosinophil-associated disorders: immunological, clinical, and molecular complexity. Semin Immunopathol 43, 423–438 (2021). [PubMed: 34052871]
82. Choudhury S, Baker S, Eosinophilic Esophagitis: the Potential Role of Biologics in its Treatment. Clin Rev Allergy Immunol, (2019).

83. Turner JA, Stephen-Victor E, Wang S, Rivas MN, Abdel-Gadir A et al. , Regulatory T Cell-Derived TGF-beta1 Controls Multiple Checkpoints Governing Allergy and Autoimmunity. Immunity 53, 1331–1332 (2020). [PubMed: 33326768]
84. Sellheyer K, Bickenbach JR, Rothnagel JA, Bundman D, Longley MA, Krieg T, Roche NS, Roberts AB, Roop DR, Inhibition of skin development by overexpression of transforming growth factor beta 1 in the epidermis of transgenic mice. Proc Natl Acad Sci USA 90, 5237–5241 (1993). [PubMed: 7685120]
85. Cheng N, Bhowmick NA, Chytil A, Gorksa AE, Brown KA et al. , Loss of TGF-beta type II receptor in fibroblasts promotes mammary carcinoma growth and invasion through upregulation of TGF-alpha-, MSP- and HGF-mediated signaling networks. Oncogene 24, 5053–5068 (2005). [PubMed: 15856015]
86. Wong CK, Leung KM, Qiu HN, Chow JY, Choi AO, Lam CW, Activation of eosinophils interacting with dermal fibroblasts by pruritogenic cytokine IL-31 and alarmin IL-33: implications in atopic dermatitis. PLoS One 7, e29815 (2012). [PubMed: 22272250]
87. Rafiee P, Ogawa H, Heidemann J, Li MS, Aslam M et al. , Isolation and characterization of human esophageal microvascular endothelial cells: mechanisms of inflammatory activation. Am J Physiol Gastrointest Liver Physiol 285, G1277–1292 (2003). [PubMed: 12919942]
88. Roan F, Obata-Ninomiya K, Ziegler SF, Epithelial cell-derived cytokines: more than just signaling the alarm. J Clin Invest 129, 1441–1451 (2019). [PubMed: 30932910]
89. Laky K, Dugan P, Frischmeyer-Guerrerio PA, Hematopoietic reconstitution of neonatal immunocompetent mice to study conditions with a perinatal window of susceptibility. Sci Rep 8, 12254 (2018). [PubMed: 30115970]
90. Nakagawa H, Kasagi Y, Karakasheva TA, Hara T, Aaron B et al. , Modeling Epithelial Homeostasis and Reactive Epithelial Changes in Human and Murine Three-Dimensional Esophageal Organoids. Curr Protoc Stem Cell Biol 52, e106 (2020). [PubMed: 32105412]
91. Sheridan BS, Lefrancois L, Isolation of mouse lymphocytes from small intestine tissues. Curr Protoc Immunol Chapter 3, Unit3 19 (2012).
92. Bolger AM, Lohse M, Usadel B, Trimmomatic: a flexible trimmer for Illumina sequence data. Bioinformatics 30, 2114–2120 (2014). [PubMed: 24695404]
93. Dobin A, Davis CA, Schlesinger F, Drenkow J, Zaleski C, Jha S, Batut P, Chaisson M, Gingeras TR, STAR: ultrafast universal RNA-seq aligner. Bioinformatics 29, 15–21 (2013). [PubMed: 23104886]
94. Li B, Dewey CN, RSEM: accurate transcript quantification from RNA-Seq data with or without a reference genome. BMC Bioinformatics 12, 323 (2011). [PubMed: 21816040]
95. Ritchie ME, Phipson B, Wu D, Hu Y, Law CW, Shi W, Smyth GK, limma powers differential expression analyses for RNA-sequencing and microarray studies. Nucleic Acids Res 43, e47 (2015). [PubMed: 25605792]
96. DeWard AD, Cramer J, Lagasse E, Cellular heterogeneity in the mouse esophagus implicates the presence of a nonquiescent epithelial stem cell population. Cell Rep 9, 701–711 (2014). [PubMed: 25373907]
97. Sato T, Stange DE, Ferrante M, Vries RG, Van Es JH et al. , Long-term expansion of epithelial organoids from human colon, adenoma, adenocarcinoma, and Barrett's epithelium. Gastroenterology 141, 1762–1772 (2011). [PubMed: 21889923]
98. Rouillard AD, Gundersen GW, Fernandez NF, Wang Z, Monteiro CD, McDermott MG, Ma'ayan A, The harmonizome: a collection of processed datasets gathered to serve and mine knowledge about genes and proteins. Database 2016, (2016).
99. Akiyoshi S, Ishii M, Nemoto N, Kawabata M, Aburatani H, Miyazono K, Targets of transcriptional regulation by transforming growth factor-beta: expression profile analysis using oligonucleotide arrays. Jpn J Cancer Res 92, 257–268 (2001). [PubMed: 11267935]
100. Koinuma D, Tsutsumi S, Kamimura N, Imamura T, Aburatani H, Miyazono K, Promoter-wide analysis of Smad4 binding sites in human epithelial cells. Cancer Sci 100, 2133–2142 (2009). [PubMed: 19686287]
101. Levy L, Hill CS, Smad4 dependency defines two classes of transforming growth factor beta (TGFβ) target genes and distinguishes TGFβ-induced epithelial-mesenchymal transition from

its antiproliferative and migratory responses. Mol Cell Biol 25, 8108–8125 (2005). [PubMed: 16135802]

102. Valcourt U, Kowanetz M, Niimi H, Heldin CH, Moustakas A, TGF-beta and the Smad signaling pathway support transcriptomic reprogramming during epithelial-mesenchymal cell transition. Mol Biol Cell 16, 1987–2002 (2005). [PubMed: 15689496]
103. Zavadil J, Bitzer M, Liang D, Yang YC, Massimi A, Kneitz S, Piek E, Bottinger EP, Genetic programs of epithelial cell plasticity directed by transforming growth factor-beta. Proc Natl Acad Sci U S A 98, 6686–6691 (2001). [PubMed: 11390996]
104. D'Souza RC, Knittle AM, Nagaraj N, van Dinther M, Choudhary C, ten Dijke P, Mann M, Sharma K, Time-resolved dissection of early phosphoproteome and ensuing proteome changes in response to TGF-beta. Sci Signal 7, rs5 (2014). [PubMed: 25056879]
105. Kang Y, Chen CR, Massague J, A self-enabling TGFbeta response coupled to stress signaling: Smad engages stress response factor ATF3 for Id1 repression in epithelial cells. Mol Cell 11, 915–926 (2003). [PubMed: 12718878]
106. Colombo I, Sangiovanni E, Maggio R, Mattozzi C, Zava S et al. , HaCaT Cells as a Reliable In Vitro Differentiation Model to Dissect the Inflammatory/Repair Response of Human Keratinocytes. Mediators Inflamm 2017, 7435621 (2017). [PubMed: 29391667]
107. Ju SM, Song HY, Lee SJ, Seo WY, Sin DH et al. , Suppression of thymus- and activation-regulated chemokine (TARC/CCL17) production by 1,2,3,4,6-penta-O-galloyl-beta-D-glucose via blockade of NF-kappaB and STAT1 activation in the HaCaT cells. Biochem Biophys Res Commun 387, 115–120 (2009). [PubMed: 19576177]
108. Groves RW, Rauschmayr T, Nakamura K, Sarkar S, Williams IR, Kupper TS, Inflammatory and hyperproliferative skin disease in mice that express elevated levels of the IL-1 receptor (type I) on epidermal keratinocytes. Evidence that IL-1-inducible secondary cytokines produced by keratinocytes in vivo can cause skin disease. J Clin Invest 98, 336–344 (1996). [PubMed: 8755642]

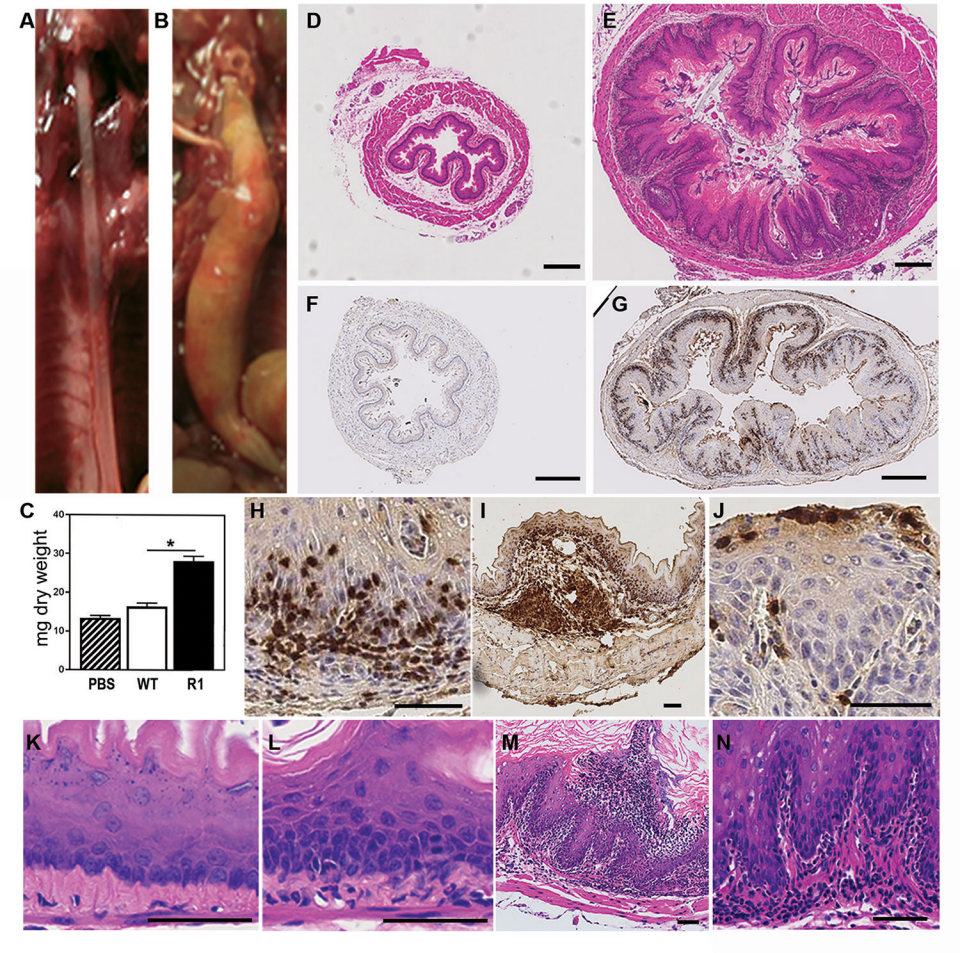

Fig 1. R1 mice spontaneously develop clinical and histological features that phenocopy human EoE.

(A, B) Gross photos of esophagi from WT (A) and R1 (B) mice show esophageal dilation and food impaction in R1 mice.

(C) Esophagi of WT or R1 mice were flushed and then the lyophilized contents were weighed. Each bar is the mean ± SEM of 5–7 mice analyzed individually.

(D, E) Cross-sections of H&E-stained esophagi from WT (D) and R1 (E) mice show dilation and inflammation in R1 mice.

(F-J). IHC for eosinophil granule major basic protein (MBP) in cross-sections of esophagi from representative WT (F) and R1 (G) mice illustrate examples of >15 eosinophils per hpf (G, H), eosinophilic micro-abscess (I) and surface layering of eosinophils (J) in R1 esophagi.

(K-N). H&E-stained tissues show basal cell hyperplasia (L), abscess (M) and rete peg expansion (E, N) in R1 mice, none of which are seen in WT esophagi (D, K).

D-G Scale bars 200μM; H-N Scale bars 50μM. Mice were ≥24 wk old.

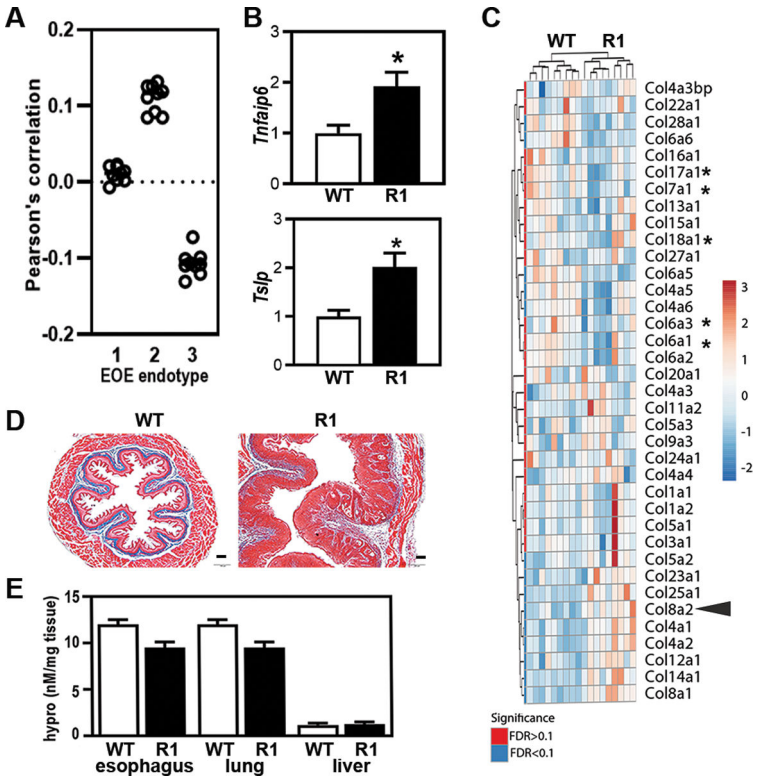

Fig 2. Transcriptional profile of R1 esophagi is consistent with EoE endotype 2.

(A) Correlation analysis of *Tgfbr1*^{M318R} mice based on gene expression of the EoE Diagnostic Panel of Shoda et al. (7). The Pearson's correlation coefficient was calculated across all 96 genes for 9 individual 16 wk old R1 mice versus the mean expression in the discovery cohort for each endotype.

(B) RNA isolated from the inner esophagus of 8–10 wk old WT and R1 mice was analyzed by RT-PCR. Data shown are the mean fold change ± SEM for N= 12 mice per group.

(C-E) R1 esophagi show no signs of fibrostenosis, a hallmark feature of EoE endotype 3.

(C) Heat map of RNA-seq expression data depicting collagen gene expression in 16 wk old R1 esophagi. The representative collagen gene in the human EoE diagnostic panel *Col8a2,* is highlighted (◄). Collagen genes whose promoter contains a SMAD binding element or have been previously demonstrated to be induced by TGFβ are marked by asterisks (*)(8, 98).

(D) WT or R1 esophagi from representative ≥24 wk old mice stained with Masson's Trichrome. Scale bars, 50 μM.

(E) Hydroxyproline content in esophagus, lung, or liver, from ≥24 wk old WT and R1 mice was quantified as an indication of collagen content. Each bar is the mean ± SEM of 5–7 mice analyzed individually. See also Fig. S1.

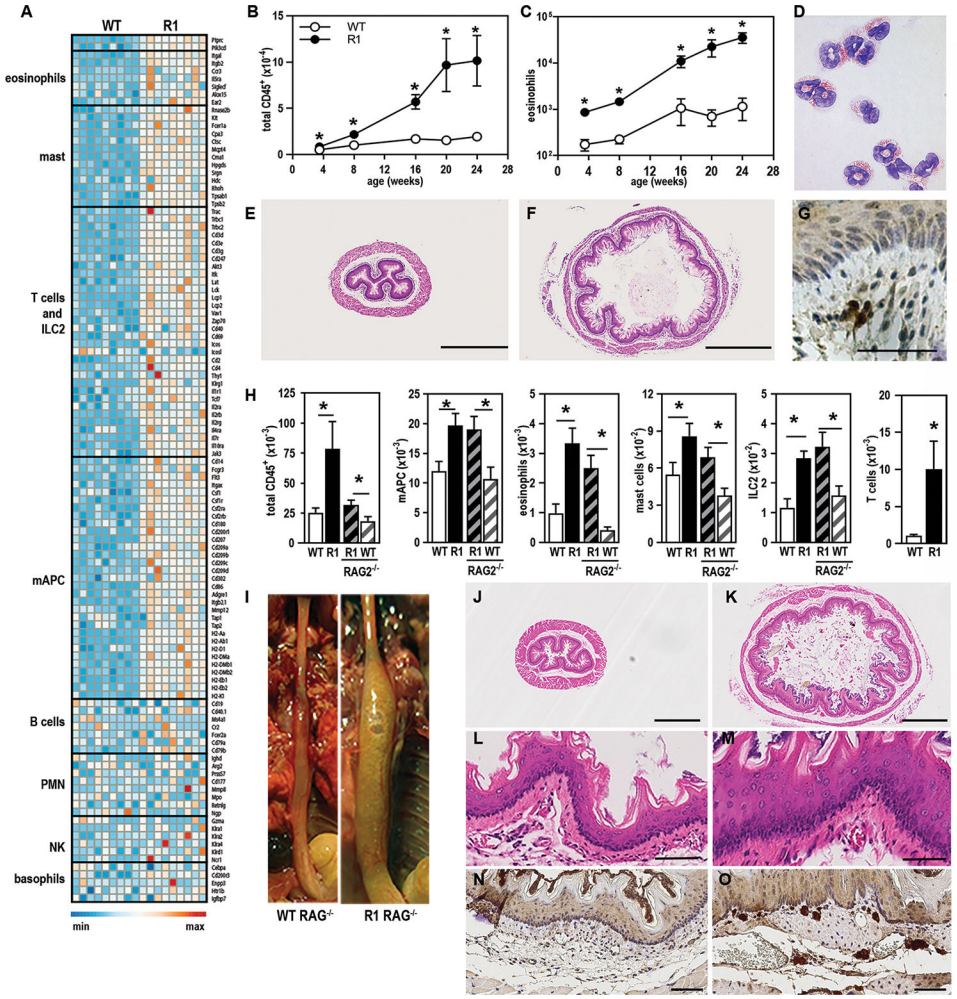

Fig. 3. R1 mice develop early onset EoE that is independent of T cells.

(A) RNASeq was performed using RNA isolated from the inner esophagus of 16 wk old WT and R1 mice. Heat map depicts the relative expression of genes characteristic of the hematopoietic cell lineages indicated.

(B-G) R1 mice develop early onset EoE with characteristics of EoEe2.

The number of total $CD45^+$ cells (B) or eosinophils (C) isolated from esophagi of 3.5–24 wk old WT and R1 mice was enumerated using flow cytometry. Each data point is the mean ± SEM of ≥7 mice per group. (D) Modified Giemsa stained cytospin of eosinophils isolated from R1 esophagi. (E, F) H&E-stained images of esophagi from 3.5 wk old WT (E) and R1 (F) weanlings. (G) IHC for MBP in the esophagus of a representative 3.5 wk old R1 weanling with >15 eosinophils per hpf.

(H) The inflammatory infiltrates isolated from esophagi of 8 wk old WT and R1 mice on RAG-sufficient and RAG-deficient backgrounds were analyzed by flow cytometry. Data are mean ± SEM of ≥14 mice per group. See also Figs. S2 and S3.

(I-O) Images of esophagi from ≥24 wk old $RAG^{-/-}$ (I, J, L, N) and $RAG^{-/-}$R1 (I, K, M, O) mice. H&E-stained sections illustrate dilation with food impaction (K) and basal cell hyperplasia (M) in $RAG^{-/-}$R1 mice. IHC for MBP^+ (N, O).

Scale bars for x-sections 500 μM (E, F, J, K); all others 50 μM.

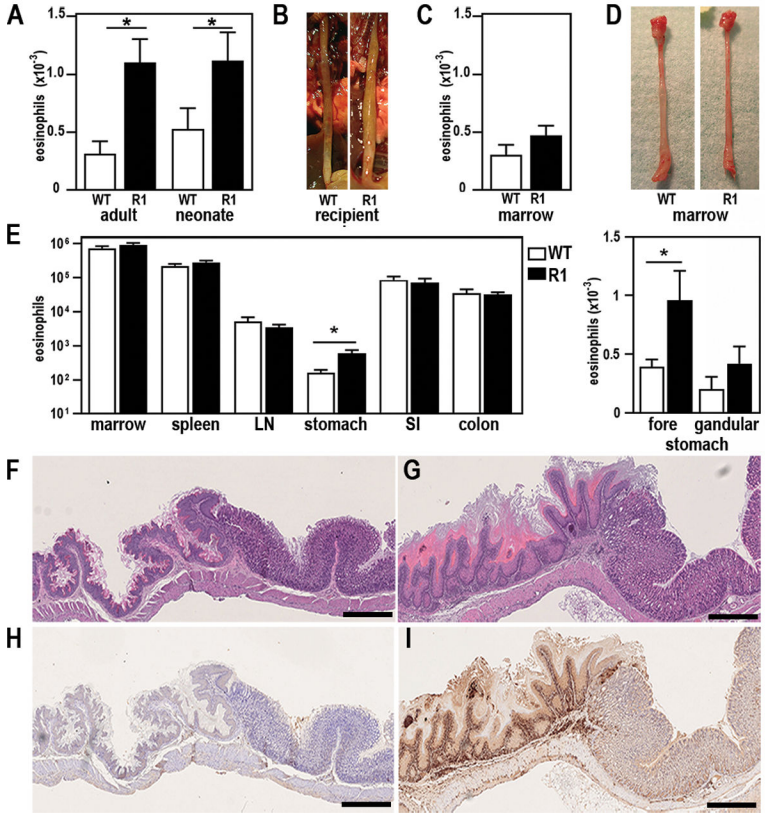

Fig. 4. Non-hematopoietic cells are necessary and sufficient to initiate allergic inflammation in esophagi of R1 mice.

(A-D) WT and R1 mice were irradiated and reconstituted with CD45-congenic WT BM as adults or neonates (A, B). Conversely, WT mice were irradiated and reconstituted with R1 BM (C, D). Eight weeks after reconstitution the number of donor BM-derived eosinophils in the esophagus was enumerated. Data are mean ± SEM of ≥8 mice per group. Gross images illustrate that only R1 mice reconstituted with WT BM developed esophageal dilation with food impaction (B).

(E-I) Features characteristic of EoE co-localize with stratified squamous epithelium. The number of eosinophils isolated from various tissues of 4–8 wk old WT and R1 mice was calculated. Data are mean ± SEM of ≥4 per group. Images of stomach from representative ≥24 wk old WT (F, H) or R1 (G, I) mice stained with H&E (F, G) or anti-MBP (H, I). Scale bars 500 μM.

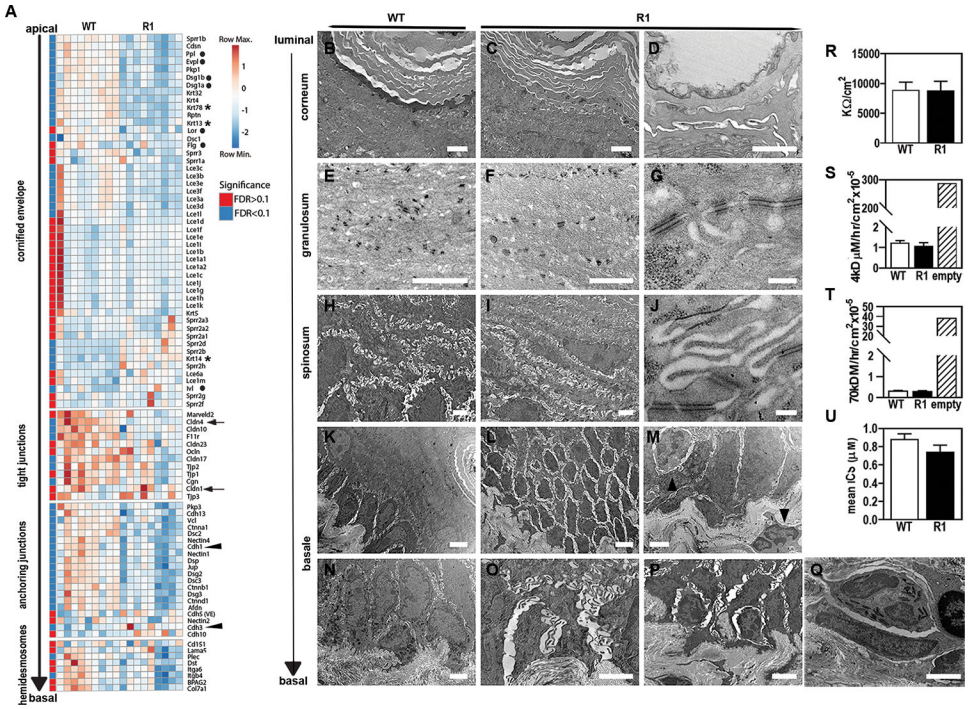

Fig. 5. No evidence of impaired barrier function in esophagi of R1 mice.

(A) Heat map of RNA-seq expression data from 16 wk old WT and R1 mice depicts relative expression of genes encoding structural proteins characteristic of each strata of epithelium. Genes associated with severe dermatitis, multiple selected developmentally regulated structural elements (●), cadherins (◄), claudins (←), and keratins (*) are highlighted.

(B-Q) Ultrastructural features of esophagi from 8–16 wk old WT and R1 mice were analyzed by transmission electron microscopy. Scale bars are 2 μM except G, J 200 nm; K, P 4 μM; L 6 μM; N 5 μM.

(R-T) Transepithelial electrical resistance (R) and paracellular permeability of 4 kD (S) or 70 kD (T) dextran through the esophageal wall of 8 wk old WT or R1 mice was measured using a Ussing Chamber. One chamber was left empty (hashed bars) to determine the maximum amount of transfer possible during the 3 h assay. Data are mean ± SEM of ≥4 mice per group.

(U) Mean distance between cell bodies of adjacent basal epithelial cells in transmission electron microscopy images of esophagi from 8–16 wk old WT and R1 mice. Data are mean ± SEM of N=15 fields scored per genotype. See also Fig S5.

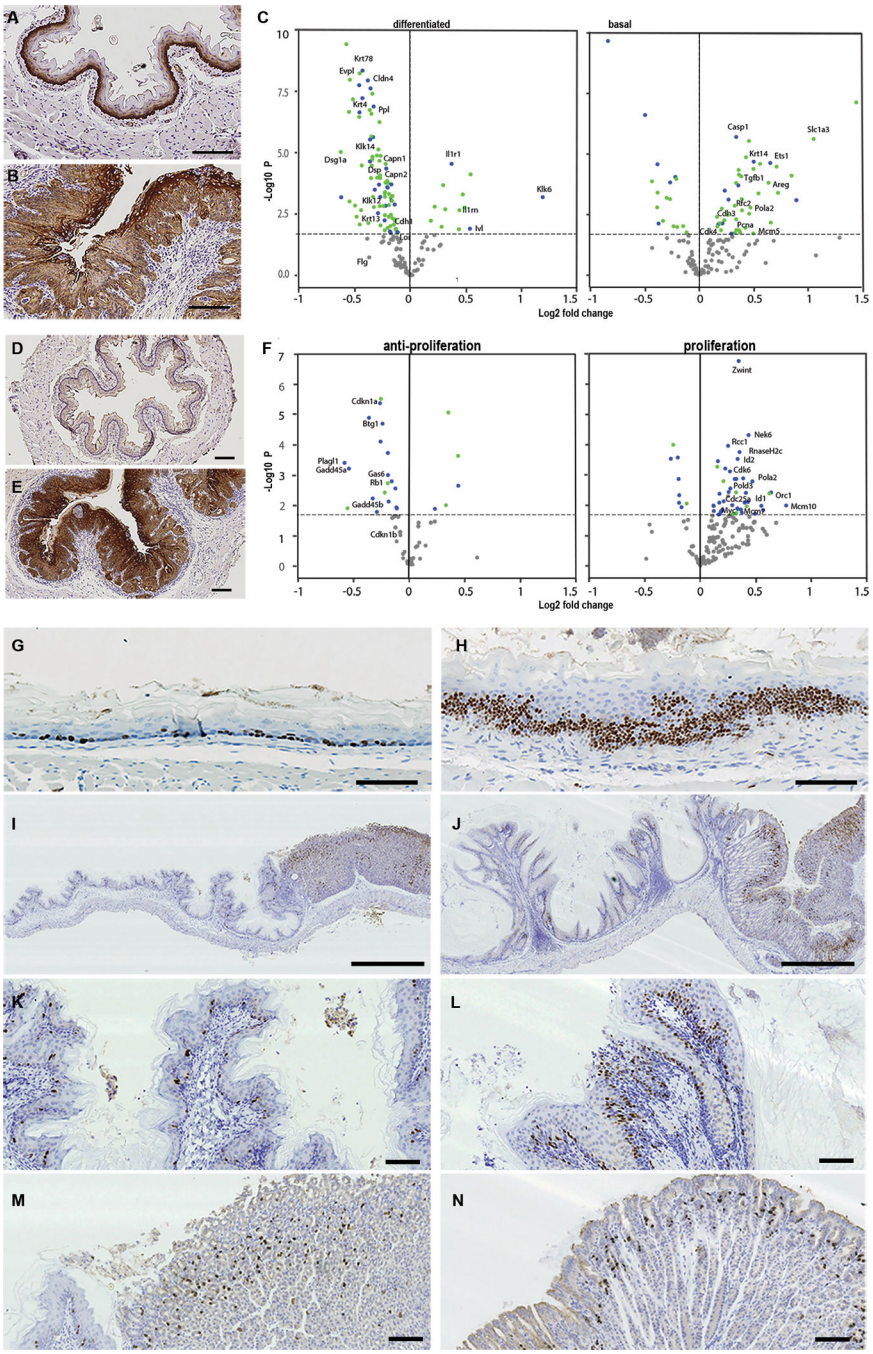

Fig. 6. R1 esophageal epithelial cells show signs of distress and excessive proliferation.

(A, B) IHC showing the expression pattern of keratin 14 in esophagi from ≥24 wk old WT (A) and R1 (B) mice.

(C) Volcano plots of RNA-seq expression data from esophagi from 16 wk old WT and R1 mice for genes differentially expressed between differentiated or basal keratinocyte genes (25). Horizontal dashed lines indicate significance (FDR<0.01). Differentially expressed genes whose promoter contains a SMAD2/3 binding element and/or have been previously reported to be transcriptionally regulated by TGFβ are blue (34, 98–103).

(D, E) IHC showing the expression of keratin 6 in esophagi of ≥24 wk old R1 (B) and WT (A) mice.

(F) Volcano plots of RNA-seq expression data from esophagi from 16 wk old WT and R1 mice for genes encoding proteins that induce cell cycle arrest or promote proliferation (28, 104, 105). Horizontal dashed lines indicate significance (FDR<0.01). Differentially expressed genes whose promoter contains a SMAD2/3 binding element or have been previously demonstrated to be subject to regulation by TGFβ are blue (28, 98, 101, 102, 104, 105).

(G-N) IHC for the thymidine-analogue BrdU in the esophagus (G, H), forestomach (I, J, K, L), and glandular stomach (I, J, M, N), of ≥20 wk old WT (G, I, K, M) and R1 (H, J, L, N) mice.

Scale bars 100 μM except I, J 1 mm.

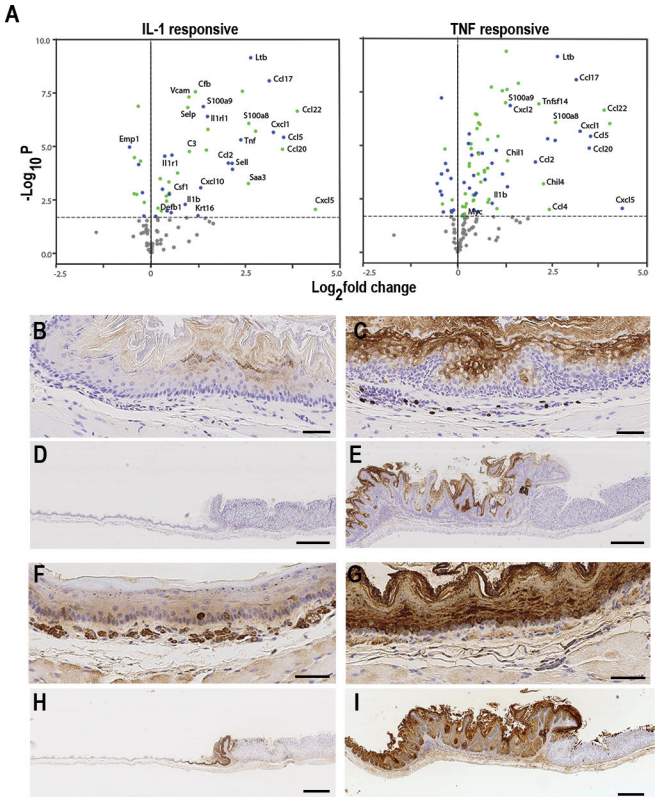

Fig. 7. R1 epithelial cells show signs of chronic activation associated with tissue-restricted inflammation.

(A) Volcano plots of RNA-seq expression data from esophagi from 16 wk old WT and R1 mice depicting genes transcriptionally regulated by IL-1 and TNFα (32, 34, 35, 37, 106–108). Horizontal dashed lines indicate significance (FDR<0.01). Differentially expressed genes whose promoter contains a SMAD2/3 binding element and/or have been previously demonstrated to be transcriptionally regulated by TGFβ are blue(98–103, 105).

(B-E) IHC staining of S100A9 in esophagi (B, C) and stomachs (D, E) of ≥24 wk old WT (B, D) and R1 (C, E) mice.

(F-I) IHC staining of eosinophil chemotactic factor like protein in esophagi (F, G) and stomachs (H, I) of ≥24 wk old WT (F, H) and R1 (G, I) mice.

Scale bars esophagus 50 μM, stomach 500 μM. See also Fig S7.

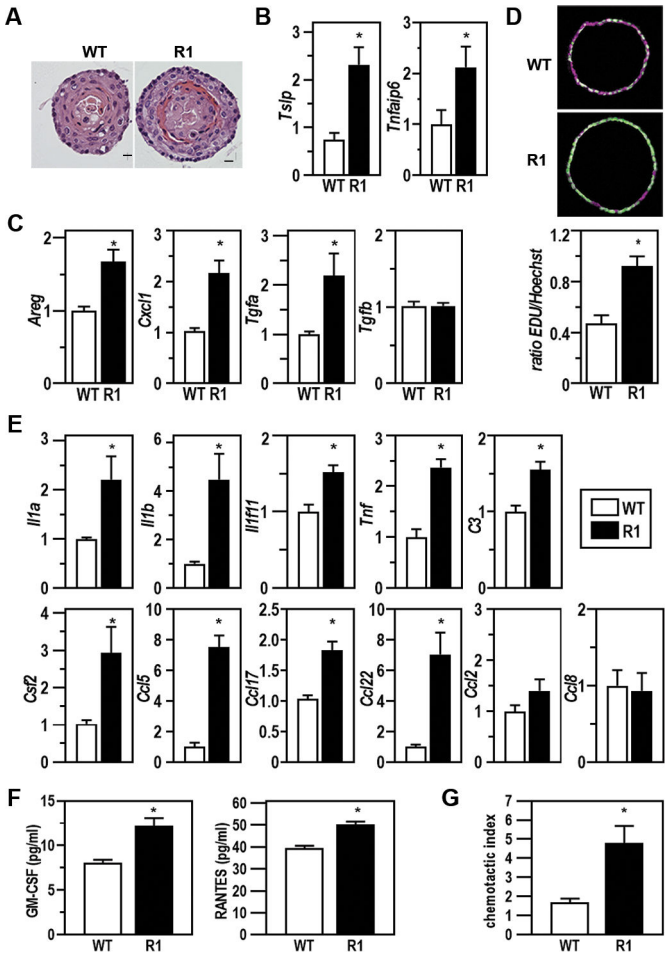

Fig. 8. Cell intrinsic changes in R1 esophageal epithelial cells drive allergic inflammation.

(A) Representative images of H&E-stained organoids generated from WT and R1 esophageal epithelial cells. Scale bars 500 μM.

(B, C) RNA isolated from WT and R1 organoids was analyzed by RT-PCR for expression of EoEe2 signature genes (B) and genes encoding epithelial growth factors (C). Each bar is the mean fold change ± SEM of 6 wells analyzed per genotype.

(D) Organoids generated from WT and R1 esophageal epithelial cells were pulsed with the thymidine analogue EdU. Nuclei were stained for EdU (green) and Hoechst33342 (purple) and then the ratios of EdU+ cells amongst total nucleated Hoechst33342+ cells were calculated. Each bar is the mean ± SEM of ≥5 wells analyzed per genotype.

(E) RNA isolated from WT and R1 organoids was analyzed by RT-PCR for expression of the genes indicated. Each bar is the mean fold change ± SEM of ≥4 wells analyzed per genotype.

(F) The concentration of RANTES and GM-CSF protein secreted by WT and R1 epithelial organoids was quantified in culture supernatants using Luminex immunoassays. Each bar is the mean ± SEM of 6 wells analyzed per genotype.

(G) Supernatants from R1 and WT organoids were added to the lower chamber of a Transwell apparatus. Eosinophils were plated in the top chamber and then allowed to

migrate for 3 h before counting. Each bar is the mean ± SEM of ≥15 wells analyzed per genotype.